



**"Dunărea de Jos" University of Galați
Doctoral School of Industrial Engineering**



ABSTRACT OF Ph.D. THESIS

Acoustic scattering on complex, rigid and elastic systems

**PhD candidate,
Ing. Necula Stan Maria**

**SCIENTIFIC COORDINATOR,
Prof. univ. dr. ing. fiz. Luminița Moraru**

Seria I 4: Inginerie industrială Nr. 83

**GALAȚI
2022**



Universitatea „Dunărea de Jos” din Galați
Școala doctorală de inginerie industrială



TEZĂ DE DOCTORAT

Împrăștierea acustică pe sisteme complexe, rigide și elastice

Doctorand

Ing. Necula Stan Maria

Președinte	Prof univ.dr.ing. Cătălin FETECĂU Președintele senatului Universitatea "Dunărea de Jos" din Galați
Conducător științific,	Prof univ.dr.ing.fiz. Luminița MORARU Director Școala Doctorală de Inginerie mecanică și industrială, Universitatea "Dunărea de Jos" din Galați
Conducător științific în cotutelă,	Prof univ.dr.ing. Eugen-Victor-Cristian RUSU Membru corespondent al Academiei Române, director CSUD - Universitatea "Dunărea de Jos" din Galați
Referenți științifici,	Prof. univ.dr.ing.Cristian-Vasile DOICIN Universitatea Politehnică București Prof.univ.dr.Gheorghe OANCEA Universitatea Transilvani Brașov Prof univ.dr.ing. habil. Antoaneta ENE Universitatea "Dunărea de Jos" din Galați

Seria I 4: Inginerie industrială Nr. 83

GALAȚI

2022

Seriile tezelor de doctorat susținute public în UDJG începând cu 1 octombrie 2013 sunt:

Domeniul fundamental ȘTIINȚE INGINEREȘTI

- Seria I 1: **Biotehnologii**
- Seria I 2: **Calculatoare și tehnologia informației**
- Seria I 3: **Inginerie electrică**
- Seria I 4: **Inginerie industrială**
- Seria I 5: **Ingineria materialelor**
- Seria I 6: **Inginerie mecanică**
- Seria I 7: **Ingineria produselor alimentare**
- Seria I 8: **Ingineria sistemelor**
- Seria I 9: **Inginerie și management în agricultură și dezvoltare rurală**

Domeniul fundamental ȘTIINȚE SOCIALE

- Seria E 1: **Economie**
- Seria E 2: **Management**
- Seria SSEF: **Știința sportului și educației fizice**

Domeniul fundamental ȘTIINȚE UMANISTE ȘI ARTE

- Seria U 1: **Filologie- Engleză**
- Seria U 2: **Filologie- Română**
- Seria U 3: **Istorie**
- Seria U 4: **Filologie - Franceză**

Domeniul fundamental MATEMATICĂ ȘI ȘTIINȚE ALE NATURII

- Seria C: **Chimie**

Domeniul fundamental ȘTIINȚE BIOLOGICE ȘI BIOMEDICALE

- Seria M: **Medicină**

THANKS

First of all, I would like to thank Prof. Dr. Eng. Luminița Moraru who accepted me into her team and offered me the chance to participate in this project and to improve my knowledge and skills; I would also like to thank her for offering me an opening in the field studied.

Special thanks go to the members of my guiding committee: Prof. Dr. Eng. Eugen-Victor-Cristian RUSU, Corresponding Member of the Romanian Academy, Prof. Dr. Eng. Antoaneta Ene and Prof. Dr. Mirela Praisler for their comments on the structure of the thesis, for their guidance during the doctoral studies and for the advice given in the final stage of the thesis.

I would also like to thank Dr. Dorin Bibicu in particular, for trusting and supporting this research project and for his interest in my work.

I especially thank everyone for helping me approach a relatively new field in my research.

I thank the management of “Dunărea de Jos” University of Galați and the Faculty of Sciences and Environment for the attention and support shown throughout the activity.

Thanks to the project Scholarships for entrepreneurship education among PhD students and postdoctoral researchers (BeAntrepreneur!), MySMIS code: 124539, which allowed me to get in touch with entrepreneurial practices and provided me with the necessary knowledge to implement a business idea related to the subject of my doctoral thesis.

Galați, 2022

Maria Necula Stan

Cuprins

THANKS	III
INTRODUCTION	5
Research Objectives	5
CHAPTER 3 SIMULATIONS OF SOUND SCATTERING BY COMPLEX BODY SYSTEMS.....	6
3.2 Mathematical models	6
3.2.1. Sound scattering by solid cylinders and spheres	6
3.4. Scattering of acoustic waves by stratified media.....	15
3.4.1. Mathematical models.....	16
CHAPTER 4 ACOUSTIC BACKSCATTERING SIMULATIONS BY TARGETS WITH COMPLEX GEOMETRIC FEATURES AND ON MULTIPLE TARGETS	27
4.1. Analysis of acoustic backscattering by non-convex kite-shape objects in the low frequency domain	27
4.2. Simulation of backscattering of acoustic waves by multiple targets - an optimization problem	31
REFERENCE LIST	40
SELECTIVE BIBLIOGRAPHY.....	42

INTRODUCTION

For several decades the problem of physical reconstruction of acoustic fields has been addressed both in the scientific community dedicated to audio communication and, more recently, by specialists studying the possible uses of low frequency acoustic waves in object detection.

Today, numerical analysis and simulation algorithms are available to the specialist allowing the use of sophisticated finite element programs, boundary elements or Fourier transforms for digital signal analysis, decomposition or reconstruction within the approximations offered by various mathematical models. All these instruments represent a complete and complex set of means for the study and description of the propagation of acoustic waves and of complex acoustic fields around objects "immersed" in the acoustic field; moreover, they enable the possibility of locating objects using techniques for reconstructing backscattered signals.

Simulation studies on the detection of "hidden" objects using low-frequency acoustic waves are the precursors to the development of a completely new and absolutely harmless technology for detecting prohibited objects (drugs or white ceramic weapons) by replacing "manual search" verification with an automated check. The most attractive and possibly fast implementation is the use of scanners in airport customs that will replace "patdown" or "hand search" verification with this automatic verification. In this way, the control process can be accelerated and "privacy and civil liberties are respected" but "the protection of citizens, society and the economy" is also effectively ensured. This emerging technology is completely harmless, and it is estimated that it will be able to detect objects hidden under clothes or in pockets without the need for contact, while maintaining the dignity and privacy of the inspected person.

In my doctoral dissertation I designed and implemented simulation experiments performed in the MATLAB environment that aimed at developing inverse scattering models in order to collect target / object information by sending sound waves towards it and by receiving and analyzing the scattered waves of the target. The inverse scattering problem is used when determining the details of the structure and composition of an object or cluster of objects that cannot be obtained from in situ measurements.

Research Objectives

While acoustic scattering experiments on solids are quite numerous in the ultrasound frequency range, acoustic scattering experiments in the range of sound frequencies are few and have not been specifically designed to detect resonances.

In order to carry out this research topic, we adapted to our simulation requirements the mathematical models that describe the scattering of a plane acoustic wave by a rigid cylinder and a rigid sphere using the whole theoretical support that describes the generation, propagation and scattering of plane waves. The properties of the object (such as structural characteristics, vibration modes, etc.) were correlated with the properties of the radiated sound field (such as the spread pressure, the remote field, or the radiation pattern of the near field, etc.). The simulations were performed by approaching the propagation of waves in the low frequency range.

Acoustic scattering events were also simulated by cylindrical and spherical targets in the double layer approach: first layer represented by air (fluid medium surrounding the target) and the second layer represented by the material of which the target is formed (sodium fluoride and chloride

sodium, PVC and steel). The multispectral distribution of the scattered signals was analyzed using the periodogram (allows estimation of the spectral density of a signal and indicates the most important frequency of oscillation in the observed time series) and 3D spectrograms (allows visual spectral density versus time).

Another research objective aimed to investigate the acoustic backscattering by non-convex objects in a two-dimensional approach. We were also interested in simulation experiments aimed at detecting and locating a finite number of targets. These were achieved using the Multiple Signal Classification (MUSIC) algorithm to collect information on the location and geometry of the distribution of targets seen as inhomogeneities in the propagation environment. MUSIC is used within two approximations. The first is the distorted-wave Born approximation (DWBA) model and it is used when the amplitude of the scattered wave is considered to be much smaller than the incident wave amplitude, and the second is the Foldy-Lax (FL) formulation of the multiple scattering model. In this study, we extend the scope of application to the low frequency range; however, the condition of homogeneity of the presumed known propagation medium remains unchanged.

Chapter 3 Simulations of sound scattering by complex body systems

3.2 Mathematical models

3.2.1. Sound scattering by solid cylinders and spheres

Although most of the solid targets on which acoustical scattering occurs can be considered rigid and immobile, this theory is limited to a few particular cases. In general, sound waves penetrating solid targets must be taken into consideration, as they have a significant effect on the angles of sound scattering and on the total energy dissipated. When a sound wave encounters an obstacle, part of the wave is reflected towards the spatial area of its original path. Scattered wave is defined as the difference between the actual wave scattered over an obstacle and the wave that will propagate undisturbed, if the obstacle does not exist in its path. Thus, when a plane wave is incident on an obstacle, in the space around the obstacle there will be, in addition to the undisturbed plane wave, a scattered wave, which is scattered from the obstacle in all directions, distorting and interfering with the incident plane wave.

Through this simulation study we are interested in estimating the wave that is scattered by a solid obstacle and the effect of this scattered wave on the sound field pressure distribution.

- I modeled a **cylinder** with a radius $a = 2$ cm. The distance between the transmitter and the investigated system is $r = 5$ cm. The fluid medium surrounding the cylinder is air with a sound velocity of $c = 343$ m/s and an average density of $\rho = 1,21$ kg/m³. A plane wave of amplitude A propagates perpendicular to the direction of the cylinder axis.

For our simulations, m is considered to be 1 and 2, and so the pressures corresponding to the incident and scattered waves, at a great distance/far from the **cylinder** become:

$$p_i = P_0 [J_0(kr) + 2i \cos(\phi) J_1(kr) - 2 \cos(2\phi) J_2(kr)] e^{-i\omega t}$$

$$p_s = A_1 \cos(\phi) [J_1(kr) + iN_1(kr)] e^{-i\omega t} + A_2 \cos(2\phi) [J_2(kr) + iN_2(kr)] e^{-i\omega t}$$

$$p_t = p_i + p_s$$

Sound scattering simulations on complex body systems

$$A_0 = -\epsilon_0 P_0 i r^{-i\gamma_0} \sin \gamma_0 \qquad A_1 = -\epsilon_1 P_0 i^2 r^{-i\gamma_1} \sin \gamma_1 = \epsilon_1 P_0 r^{-i\gamma_1} \sin \gamma_1$$

$$A_2 = -\epsilon_2 P_0 i^3 r^{-i\gamma_2} \sin \gamma_2 = \epsilon_2 P_0 i r^{-i\gamma_2} \sin \gamma_2, \quad \epsilon_m = 2, \forall m > 0$$

$$\gamma_0 = \tan^{-1} \left(-\frac{J_1(ka)}{N_1(ka)} \right) \quad \gamma_1 = \tan^{-1} \left(\frac{J_0(ka) - J_2(ka)}{N_2(ka) - N_0(ka)} \right) \quad \gamma_3 = \tan^{-1} \left(\frac{J_1(ka) - J_3(ka)}{N_3(ka) - N_1(ka)} \right)$$

γ_1, γ_2 și γ_3 are defined above.

The frequencies range was from 20 Hz to 10,000 Hz and it have been split into frequency bands (usually a 2000 Hz bandwidth) for more efficient simulation.

Moreover, for the same simulation conditions, noise was added to track the actual propagation conditions.

- We modeled a **sphere** of radius $a = 2$ cm. The fluid medium surrounding the sphere is the air through which the speed of sound propagation is $c = 343$ m/s and the average density $\rho = 1,21$ kg/m³. A plane wave of amplitude A that propagates along the +z axis axis is scattered by the rigid sphere centered at the origin (0; 0; 0). For our simulation purposes, all series in equation (3.59) are truncated to the integer value m equal to 0, 1 and 2, , and so the pressure of the wave scattered from a rigid sphere of radius a becomes:

$$p_s = -A \{ [i e^{-i\delta_0} \sin \delta_0 P_0(\cos\theta) [j_0(kr) + in_0(kr)] + 3i^2 e^{-i\delta_1} \sin \delta_1 P_1(\cos\theta) [j_1(kr) + in_1(kr)] + 5i^3 e^{-i\delta_2} \sin \delta_2 P_2(\cos\theta) [j_2(kr) + in_2(kr)]] \} e^{-i\omega t} \quad (3.66)$$

The resonant filter returns better simulation results than the other filters associated with the Helmholtz resonator, even when the signal is a noisy one. For this reason, we will limit the subsequent simulations only to the use of the resonant filter.

Frequency band 20-2000 Hz

$$Fs = 10000;$$

$$fr = [20: 10: 2000];$$

$$Fstop1 = [5 500 995 1490];$$

$$Fpass1 = [10 505 1000 1495];$$

$$Fpass2 = [3052510201515];$$

$$Fstop2 = [3553010251520];$$

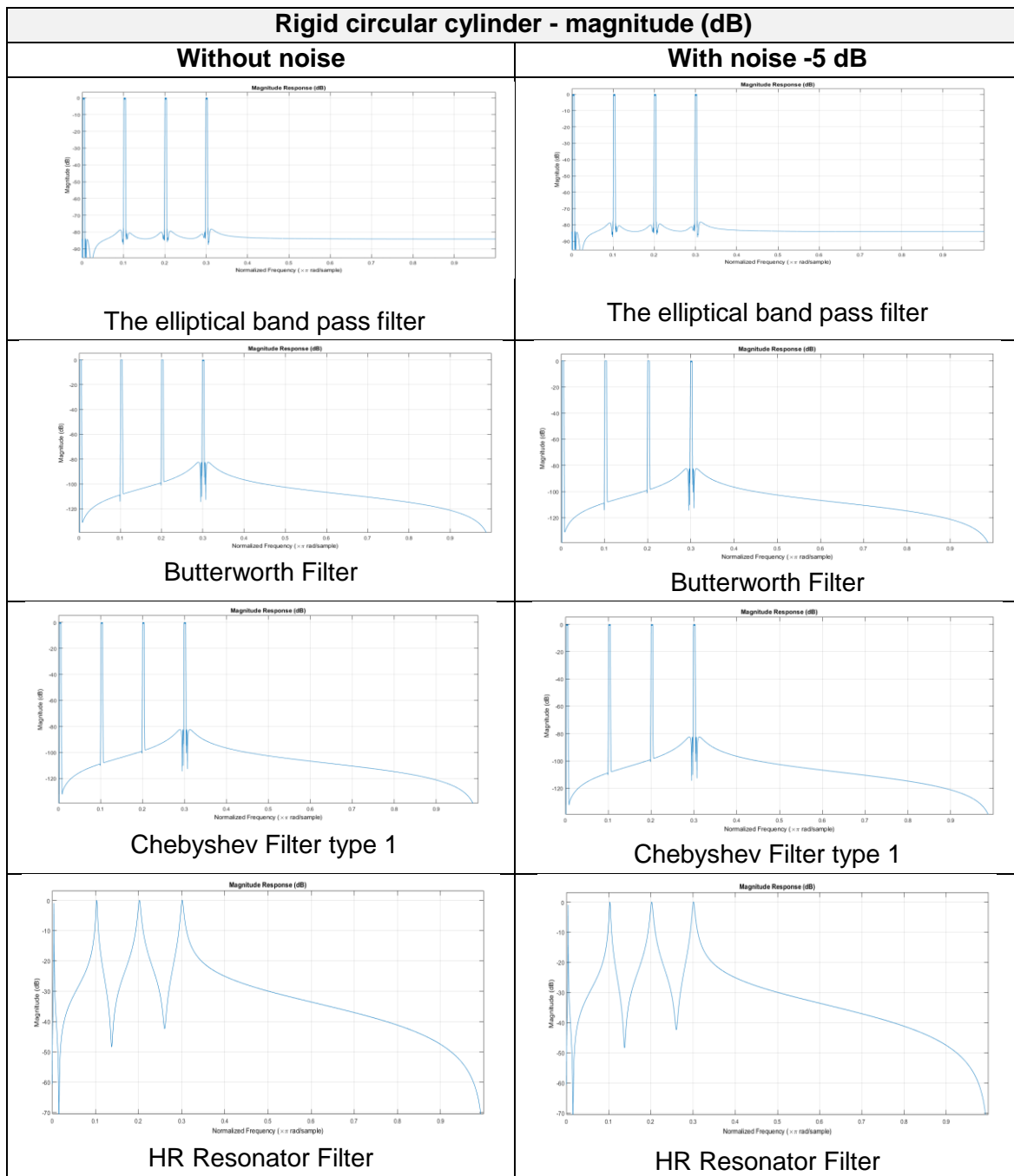
$$Astop1 = 80;$$

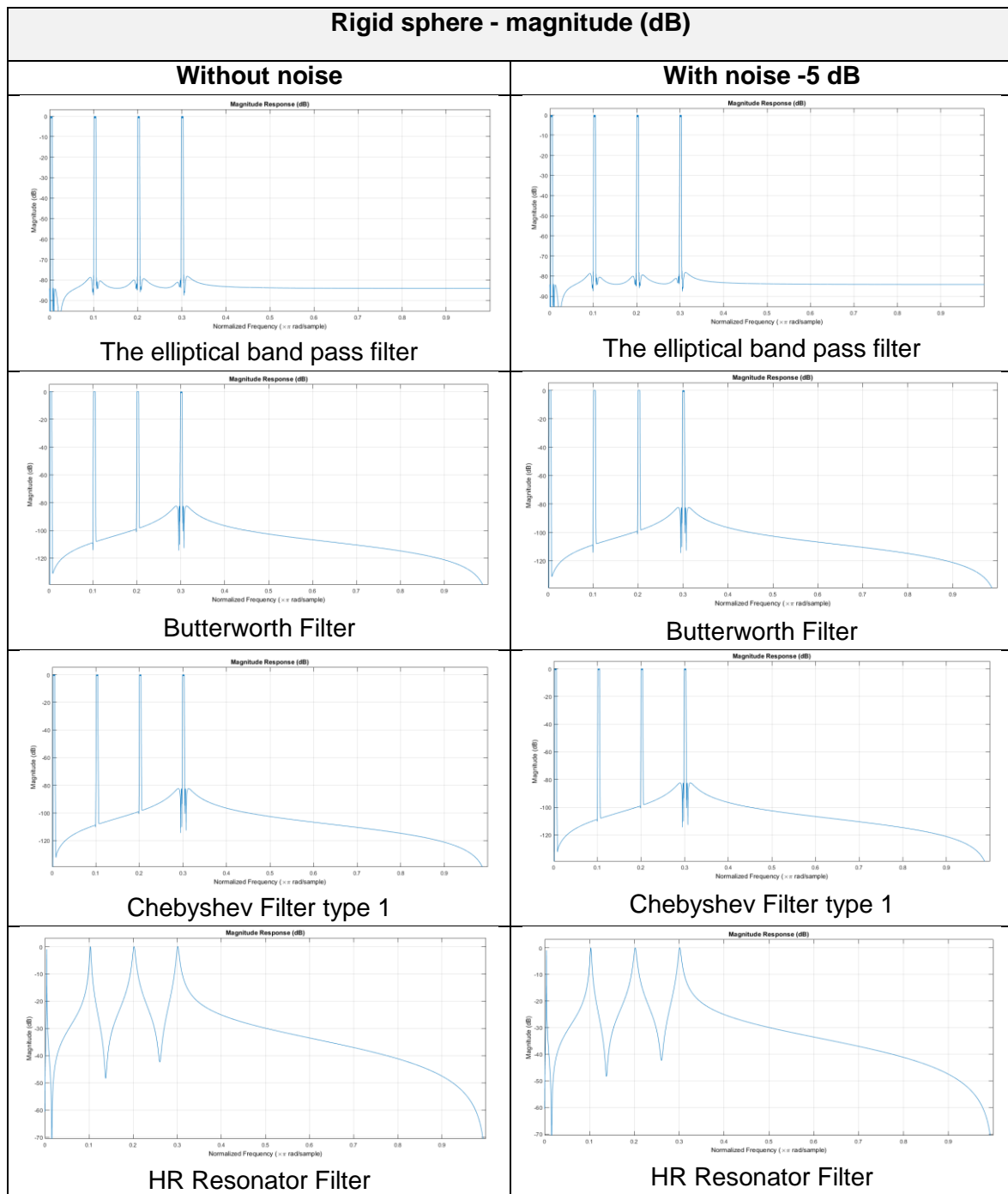
$$Astop2 = 80;$$

$$APASS = 1;$$

$$\text{For the Resonator Filter: } fr1 = 20, fr2 = 515,$$

$$fr3 = 1010, fr4 = 1505$$





A comparison between the results of simulations on the multispectral distribution of signals scattered by cylindrical and spherical objects has been made using the periodogram representation (utilized to describe and identify the dominant cycles in a particular time series) and a spectrogram (i.e. a visual representation of the spectrum) of frequency / power (Hz / dB) of the sound wave, as they vary with time).

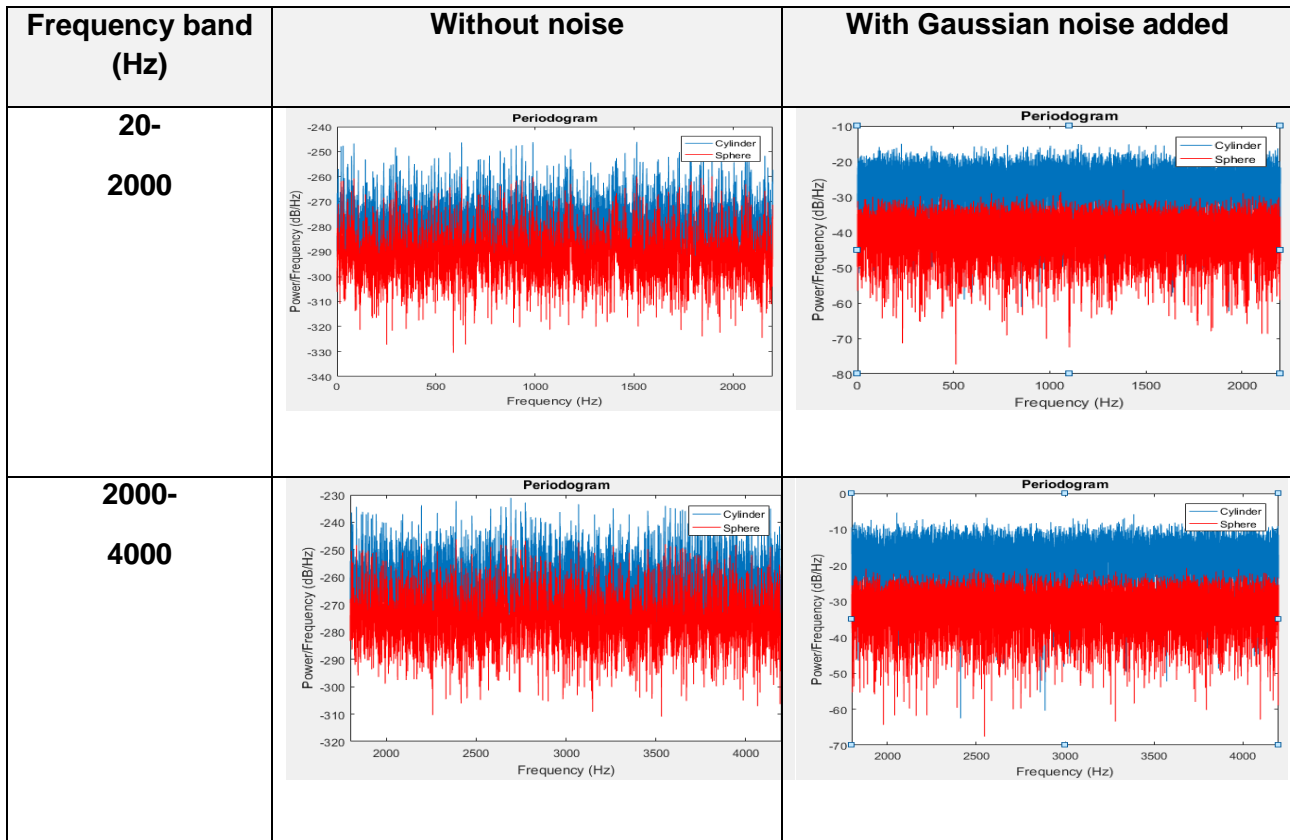
Sound scattering simulations on complex body systems

A periodogram allows the identification of important frequencies in a time series. A time series is viewed as a sum of cosine waves with varying amplitudes and frequencies. A relatively high value in the periodogram indicates the most important frequency of the oscillation in the observed time series.

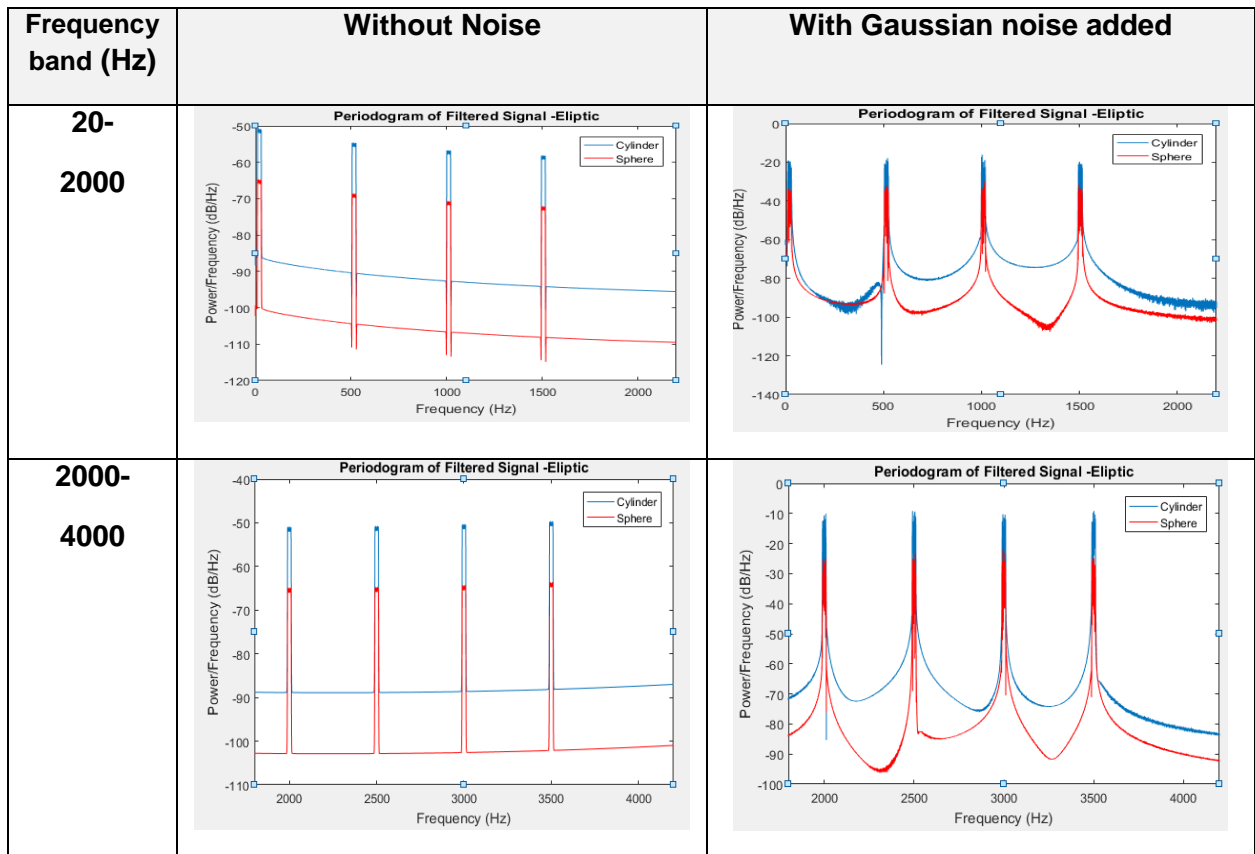
A spectrogram shows how the frequency content of a signal changes over time. It is a visual representation of a Short-Time Fourier Transform. A time series signal is divided into strips / windows. Each band is characterized by an associated frequency distribution. A local Fourier transform is applied to each band and a multitude of frequency components are obtained. The collection of all these frequency components from each band and the graphical representation of all of them is the spectrogram. Thus, it is possible to visualize signals with a wide spectrum of frequencies.

3D spectrograms are representations of intensity that depend on of frequency and time. These representations help the recognition process. The peaks correspond to different acoustic resonant frequencies. Narrowband spectrograms indicate changes in frequency / frequency response and the effect of decomposition.

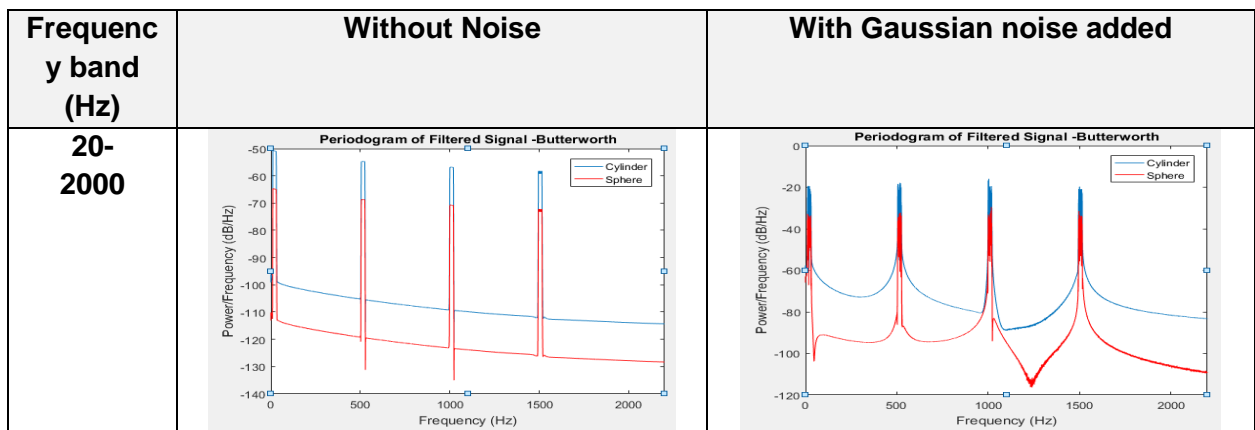
Full spectrum periodograms for cylinders and rigid spheres



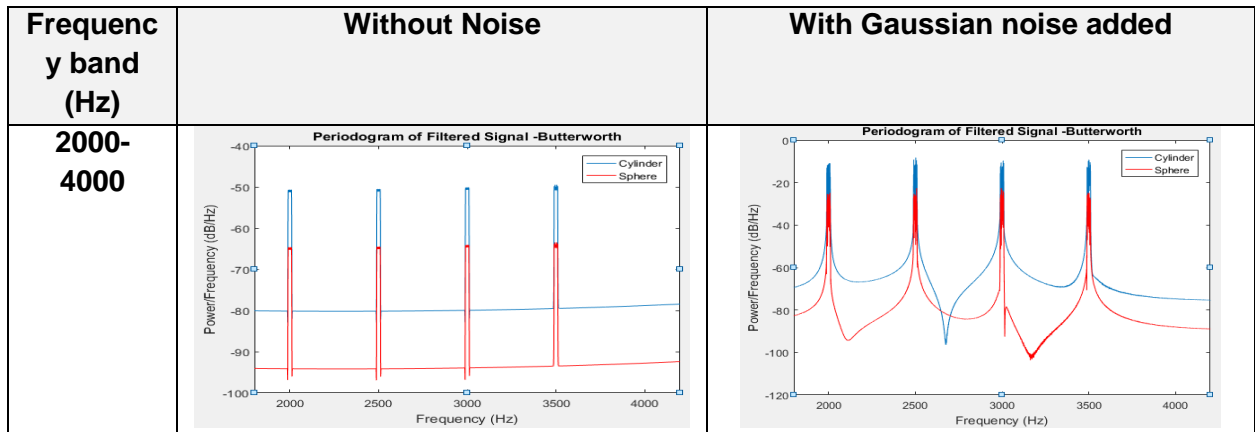
Periodograms for cylinders and rigid spheres for signals filtered with the Elliptical band pass filter



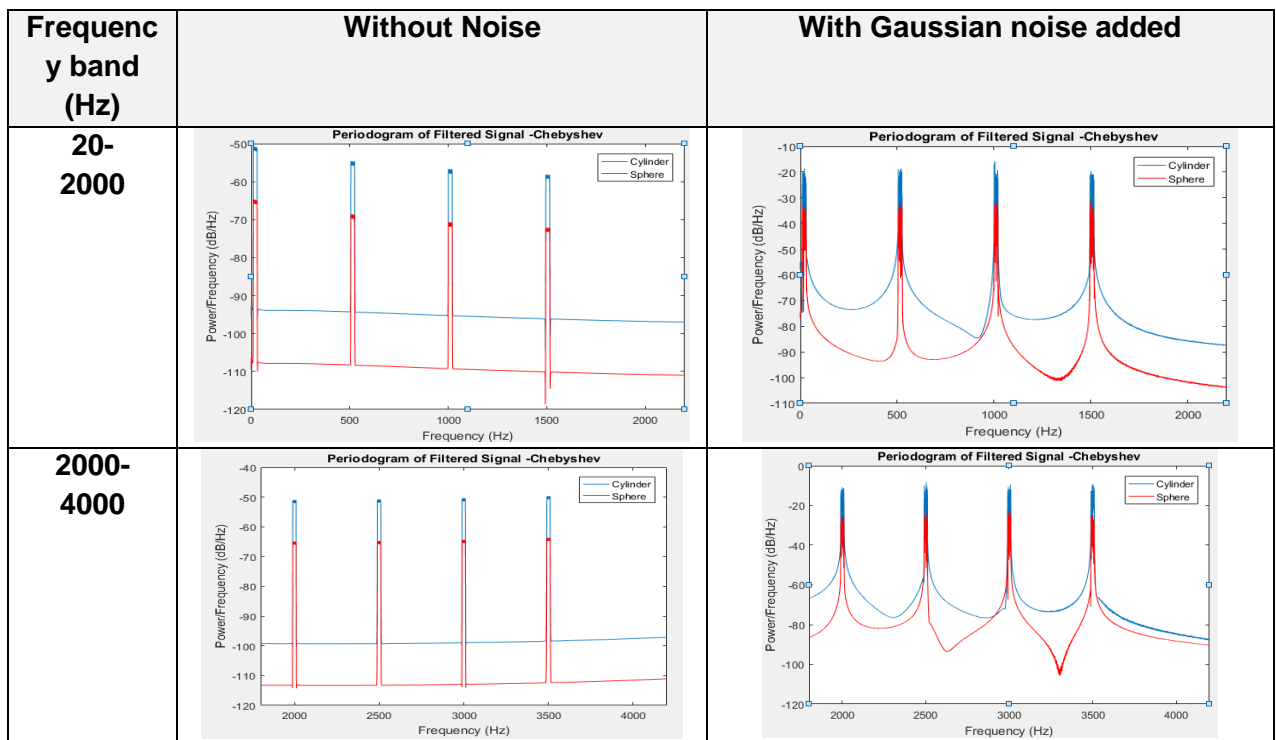
Periodograms for cylinders and rigid spheres for signals filtered with the Butterworth filter



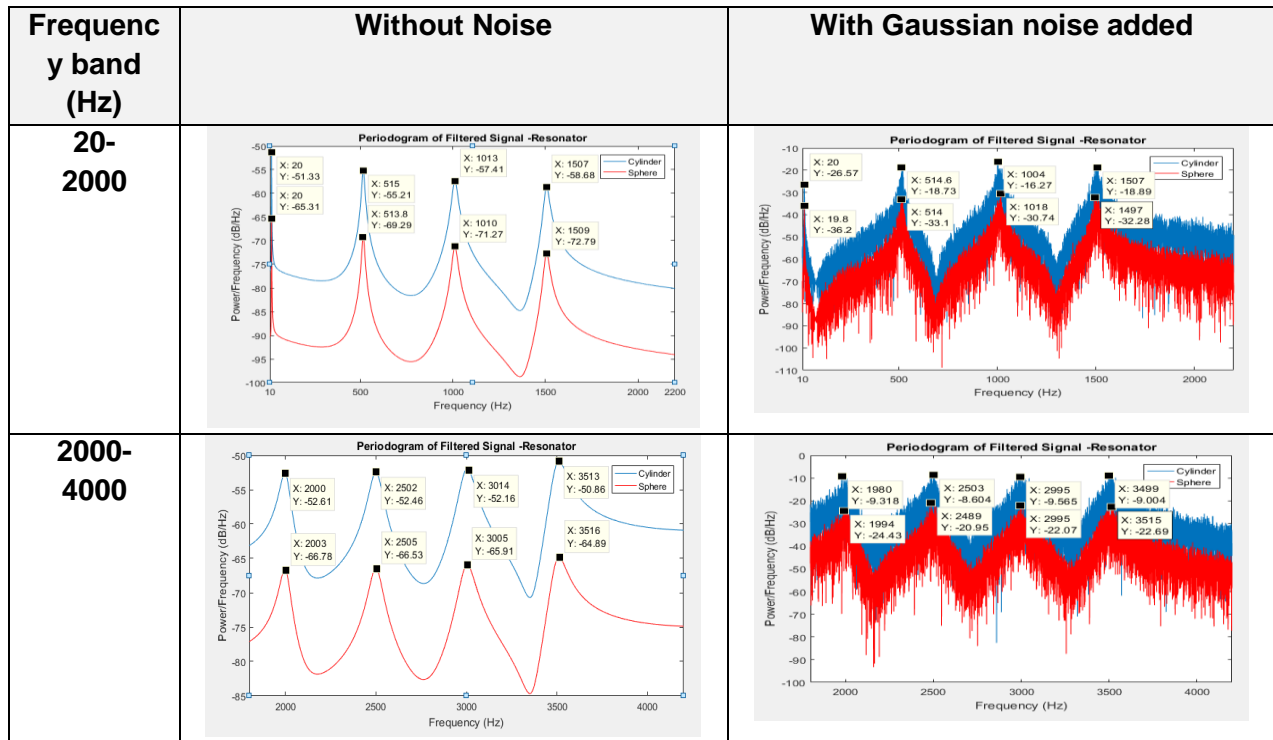
Sound scattering simulations on complex body systems



Periodograms for cylinders and rigid spheres for signals filtered with Chebyshev Type I filter



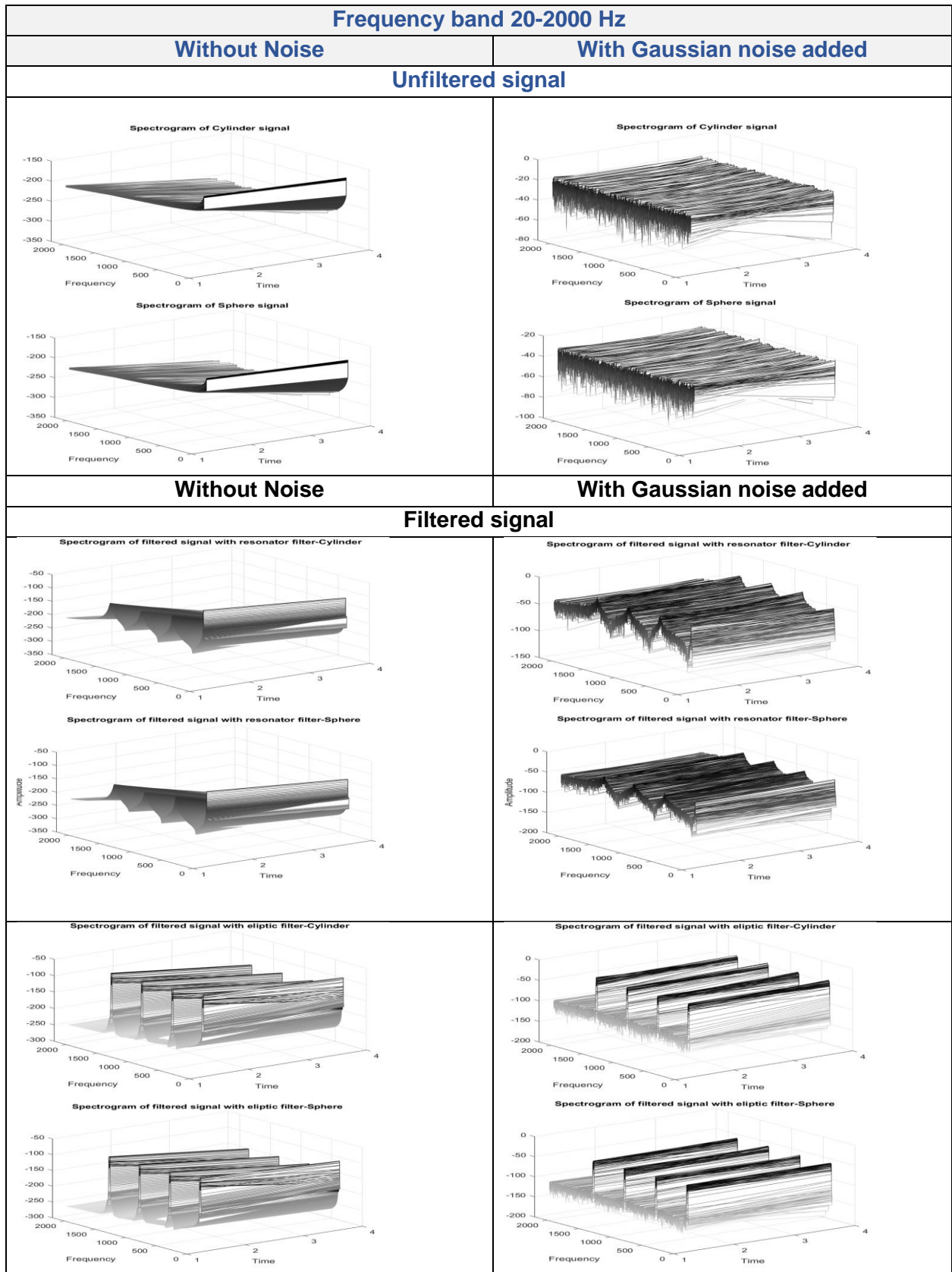
Periodograms for cylinders and rigid spheres for signals filtered with the Resonator filter

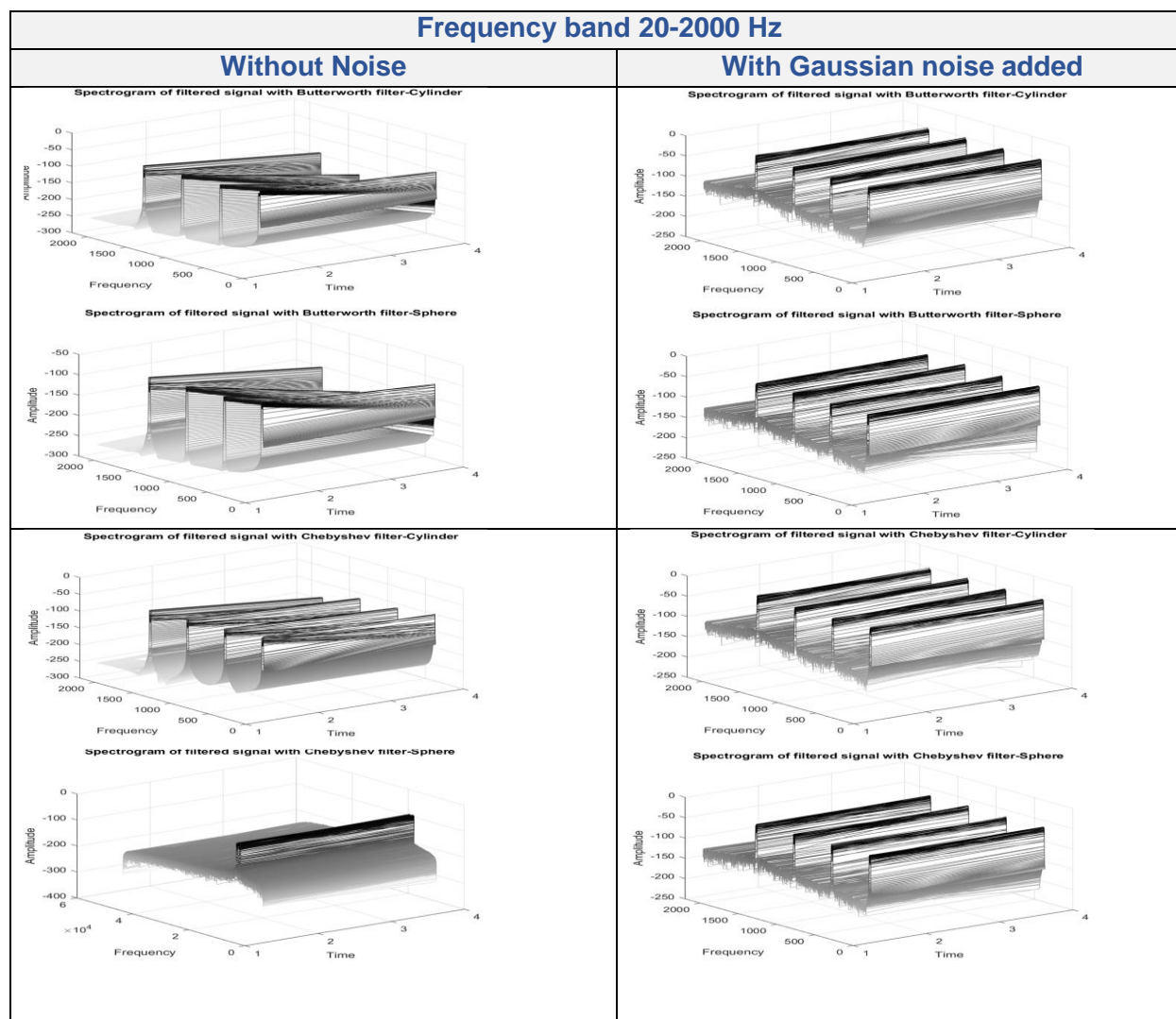


From the analysis of the multispectral distribution of the scattered signals using periodograms we conclude the following:

- Periodograms estimate the power spectrum of scattered signals and allow useful information to be extracted from available data. They visualize the variation (energy) of a signal as a function of frequency and it is observed that they have a large variation in amplitude. In other words, it shows how often these variations are important and for what frequencies these variations are weak. The most important pitch frequencies in the time range observed for the 20 Hz to 4000 Hz frequency band are $f_1 = 20$ Hz; 515 Hz; 1013 Hz și 1507 Hz.
- the power / frequency ratio is between -50 dB and -75 dB (for the cylinder) and -65 dB to -90 dB for the sphere. These values were collected in the simulations performed and indicate that the processed signals have a low signal-to-noise ratio, remaining clearly defined in the background of the noisy signals.

3D spectrograms for signals scattered on cylinders and rigid spheres and for used filters





3D spectrograms give us the following information:

- Peaks correspond to the different acoustic resonance frequencies. Narrowband spectrograms indicate changes in frequency / frequency response and attenuation effect.
- Horizontal bands, dark and evenly distributed, represent the contribution of harmonics to the scattered signal.
- For the 20-2000 Hz and 2000-4000 Hz frequency bands, the resonator filter shows the well-represented absorption bands and does not introduce the change in frequency response of the scattered signal.

3.4. Scattering of acoustic waves by stratified media

A sound wave is spread not only by a solid object, but also by objects that, in addition to acoustic properties such as density or compressibility, they also have elastic properties that can manifest in the surface layers or in the volume of the object. In the previous section we simulated the frequency response of acoustic waves scattered by **rigid** cylindrical and spherical objects. In this subchapter, our research interest is extended to the scattering of

waves by solid objects, for which we will consider their behavior at the action of shear and compression waves. Some of the acoustic energy enters the scatter in the form of shear and compression waves. On the surface of the object appear small oscillations that have an important effect on the distribution of acoustic energy in the scattered field, namely, changes in the scattering angle but also, in the total energy distribution of the scattered waves [119]. The multispectral distribution of scattered acoustic waves is a good predictor for the acoustic analysis of scattering objects. The experimental investigation was based on the simulation of scattering objects of cylindrical and sphere shape composed of two layers of materials with different elastic properties and is based on the simulation of the effects generated inside and outside the scatteres.

3.4.1. Mathematical models

The Helmholtz representation states that any continuously differentiated vector \mathbf{u} can be represented as the sum of an irrotational vector field and a solenoid vector field:

$$\mathbf{u} = -\nabla\Psi + \Delta \times \mathbf{A} \quad (3.70)$$

In other words, the displacement \mathbf{u} is composed of two terms, one associated with compression waves and the other with shear waves. Both potentials satisfy the wave equation, i.e.:

$$\nabla^2\Psi = \frac{1}{c_1^2} \frac{\partial^2\Psi}{\partial t^2} \quad (3.71a)$$

$$\nabla^2 A = \frac{1}{c_2^2} \frac{\partial^2 A}{\partial t^2} \quad (3.71b)$$

For a **cylindrical coordinate system**, $x = r \cos \theta$, $y = r \sin \theta$, $z = z$, we can consider that the defined system has a symmetry related to displacement and pressure around $\theta = 0$ (positive direction of Ox), and then the solution of ec. (3.71a) is:

$$\Psi = \sum_{n=0}^{\infty} a_n J_n(k_1 r) \cos n\theta \cdot e^{i\omega t} \quad (3.72)$$

The equation (3.71b) cannot have components in the r or θ directions, and so its solution is:

$$A_z = \sum_{n=0}^{\infty} b_n J_n(k_2 r) \sin n\theta \cdot e^{i\omega t} \quad (3.73)$$

The components of displacement (compression and shear) in solid are:

$$u_r = \sum_{n=0}^{\infty} \left[\frac{nb_n}{r} J_n(k_2 r) - a_n \frac{d}{dr} J_n(k_1 r) \right] \cos n\theta \quad (3.74)$$

$$u_\theta = \sum_{n=0}^{\infty} \left[\frac{na_n}{r} J_n(k_1 r) - b_n \frac{d}{dr} J_n(k_2 r) \right] \sin n\theta \quad (3.75)$$

And the deformation / expansion is:

$$\Delta = k_1^2 \sum_{n=0}^{\infty} a_n J_n(k_1 r) \cos n\theta \quad (3.76)$$

In the layer of air adjacent to the solid (and surrounding the solid object) the wave equation is:

$$\nabla^2 p = \frac{1}{c_3^2} \frac{\partial^2 p}{\partial t^2} \quad (3.77)$$

We assume that a plane incident wave is moving to the right along the polar axis of a sphere, of radius a , centered at the origin of the chosen coordinate system. The sphere has isotropic characteristics. In spherical coordinates, the incident wave propagates along the axis characteristic of the angle Φ . The non-zero components of the potential vector are A_Φ . In this case, the scalar and vector potentials are as follows:

$$\Psi = \sum_{n=0}^{\infty} a_n j_n(k_1 r) P_n(\cos\theta) \quad (3.89)$$

and

$$A_\Phi = \sum_{n=0}^{\infty} b_n j_n(k_2 r) \frac{d}{d\theta} P_n(\cos\theta) \quad (3.90)$$

The incident wave is written so:

$$p_i = P_0 e^{-ik_3(r\cos\theta - ct)} = P_0 \sum_{n=0}^{\infty} (2n+1)(-i)^n P_n(\cos\theta) j_n(k_3 r) e^{-i\omega t} \quad (3.91)$$

The resulting scattered acoustic waves are of the form:

$$p_s = P_0 \sum_{n=0}^{\infty} c_n P_n(\cos\theta) [j_n(k_3 r) - in_n(k_3 r)] e^{-i\omega t} \quad (3.92)$$

The same boundary conditions apply to the surface of the sphere and to the spherical coordinates:

- The air pressure (i.e. in the layer surrounding the sphere) must be equal to the normal component of the pressure from the solid to the interface;
- The radial component of the displacement in the fluid / air layer must be equal to the radial component of the displacement of the solid at the interface;
- The tangential component of the shear stress must be terminated at the surface of the solid.

Using the same method as in the case of scattering on cylindrical objects, we will have to determine the series coefficient:

$$c_n = -P_0 (2n+1)(-i)^{n+1} \sin \eta_n e^{i\eta_n} \quad (3.93)$$

Where the variation of the η_n phase for the n -th scattered wave is:

$$\tan \eta_n = \tan \delta_n(x_3) \frac{[\tan \Phi_n + \tan \alpha_n(x_3)]}{\tan \Phi_n + \tan \beta_n(x_3)} \quad (3.94)$$

Simulation parameters for acoustic scattering by cylindrical dispersing objects composed of two layers of materials with different elastic properties

In the performed simulations, the value of the integer n was truncated to 0, 1 and 2.

The conditions, conditionalities and simulation parameters are presented below.

$$p_s = \{c_0 [J_0(k_3 r) - iN_0(k_3 r)] + c_1 [J_1(k_3 r) - iN_1(k_3 r)] \cos \theta + c_2 [J_2(k_3 r) - iN_2(k_3 r)] \cos 2\theta\} e^{-i\omega t}$$

$$c_0 = -P_0 \epsilon_0 (-i) \sin \eta_0 e^{i\eta_0} = P_0 i \sin \eta_0 e^{i\eta_0}$$

$$c_1 = -P_0 \epsilon_1 (-i)^2 \sin \eta_1 e^{i\eta_1} = 2P_0 \sin \eta_1 e^{i\eta_1}$$

$$c_2 = -P_0 \epsilon_2 (-i)^3 \sin \eta_2 e^{i\eta_2} = -2P_0 i \sin \eta_2 e^{i\eta_2}$$

$$\epsilon_0 = 1 \text{ și } \epsilon_m = 2, \forall m > 0.$$

$c_0 = P_0 i \sin \eta_0 e^{i\eta_0}$	
$\tan \eta_0 = \tan \delta_0(x_3) \cdot \frac{\tan \Phi_0 + \tan \alpha_0(x_3)}{\tan \Phi_0 + \tan \beta_0(x_3)}$	$\delta_0(x_3) = \tan^{-1} \left[-\frac{J_0(x_3)}{N_0(x_3)} \right]$

	$\alpha_0(x_3) = \tan^{-1} \left[-\frac{x_3 J'_0(x_3)}{J_0(x_3)} \right]$ $= \tan^{-1} \left[\frac{x_3 J_1(x_3)}{J_0(x_3)} \right]$
	$\beta_0(x_3) = \tan^{-1} \left[-\frac{x_3 N'_0(x_3)}{N_0(x_3)} \right]$ $= \tan^{-1} \left[\frac{x_3 N_1(x_3)}{N_0(x_3)} \right]$
$\tan \Phi_0 = -\frac{\rho_3}{\rho_1} \tan \zeta_0(x_1, \sigma)$ $\zeta_0(x_1, \sigma) = \tan^{-1} \left[-\frac{x_2^2 \frac{x_1 J'_0(x_1)}{x_1 J'_0(x_1) - J_0(x_1)}}{2 \frac{\sigma}{1-2\sigma} x_1^2 [J_0(x_1) - J''_0(x_1)]} \frac{x_1 J'_0(x_1) - J_0(x_1)}{x_1 J'_0(x_1) - J_0(x_1)} \right]$ $J''_0(x) = \frac{1}{4} [J_{-2}(x) - 2J_0(x) + J_2(x)] = \frac{1}{4} [(-1)^2 J_2(x) - 2J_0(x) + J_2(x)] = \frac{1}{2} [J_2(x) - J_0(x)]$ <p>Unde $x_1 = k_1 a = \frac{2\pi v}{c_1} a$; $x_2 = k_2 a = \frac{2\pi v}{c_2} a$; și $x_3 = k_3 a = \frac{2\pi v}{c_3} a$</p> $c_1 = \sqrt{\frac{E(1-\sigma)}{\rho_1(1+\sigma)(1-2\sigma)}} \quad c_2 = \sqrt{\frac{E}{2\rho_1(1+\sigma)}} \quad c_3 = 343 \frac{m}{s}$	
$c_1 = 2P_0 \sin \eta_1 e^{i\eta_1}$	
$\tan \eta_1 = \tan \delta_1(x_3) \cdot \frac{\tan \Phi_1 + \tan \alpha_1(x_3)}{\tan \Phi_1 + \tan \beta_1(x_3)}$	$\delta_1(x_3) = \tan^{-1} \left[-\frac{J_1(x_3)}{N_1(x_3)} \right]$
	$\alpha_1(x_3) = \tan^{-1} \left[-\frac{x_3 J'_1(x_3)}{J_1(x_3)} \right]$
	$\beta_1(x_3) = \tan^{-1} \left[-\frac{x_3 N'_1(x_3)}{N_1(x_3)} \right]$
$\tan \Phi_1 = -\frac{\rho_3}{\rho_1} \tan \zeta_1(x_1, \sigma)$	
$\zeta_1(x_1, \sigma) = \tan^{-1} \left[-\frac{x_2^2 \frac{x_1 J'_1(x_1)}{x_1 J'_1(x_1) - J_1(x_1)} - \frac{2J_1(x_2)}{J_1(x_2) - x_2 J'_1(x_2) + x_2^2 J''_1(x_2)}}{2 \frac{\sigma}{1-2\sigma} x_1^2 [J_1(x_1) - J''_1(x_1)]} \frac{x_1 J'_1(x_1) - J_1(x_1)}{x_1 J'_1(x_1) - J_1(x_1)} + \frac{2[x_2 J'_1(x_2) - J_1(x_2)]}{J_1(x_2) - x_2 J'_1(x_2) + x_2^2 J''_1(x_2)} \right]$ <p>unde $x_1 = k_1 a = \frac{2\pi v}{c_1} a$; $x_2 = k_2 a = \frac{2\pi v}{c_2} a$; și $x_3 = k_3 a = \frac{2\pi v}{c_3} a$</p> $c_1 = \sqrt{\frac{E(1-\sigma)}{\rho_1(1+\sigma)(1-2\sigma)}} \quad c_2 = \sqrt{\frac{E}{2\rho_1(1+\sigma)}} \quad c_3 = 343 \frac{m}{s}$	
$c_2 = -2P_0 i \sin \eta_2 e^{i\eta_2}$	
$\tan \eta_2 = \tan \delta_2(x_3) \cdot \frac{\tan \Phi_2 + \tan \alpha_2(x_3)}{\tan \Phi_2 + \tan \beta_2(x_3)}$	$\delta_2(x_3) = \tan^{-1} \left[-\frac{J_2(x_3)}{N_2(x_3)} \right]$
	$\alpha_n(x_3) = \tan^{-1} \left[-\frac{x_3 J'_2(x_3)}{J_2(x_3)} \right]$

	$\beta_n(x_3) = \tan^{-1} \left[-\frac{x_3 N'_2(x_3)}{N_2(x_3)} \right]$
$\tan \Phi_2 = -\frac{\rho_3}{\rho_1} \tan \zeta_2(x_1, \sigma)$	
$\zeta_2(x_1, \sigma) = \tan^{-1} \left[-\frac{x_2^2 \frac{x_1 J'_2(x_1)}{x_1 J'_2(x_1) - J_2(x_1)} \frac{8 J_2(x_2)}{4 J_2(x_2) - x_2 J'_2(x_2) + x_2^2 J''_2(x_2)}}{2 \frac{\sigma}{1-2\sigma} \frac{x_1^2 [J_2(x_1) - J'_2(x_1)]}{x_1 J'_2(x_1) - J_2(x_1)} + \frac{8 [x_2 J'_2(x_2) - J_2(x_2)]}{4 J_2(x_2) - x_2 J'_2(x_2) + x_2^2 J''_2(x_2)}} \right]$	
$\text{unde } x_1 = k_1 a = \frac{2\pi\nu}{c_1} a; \quad x_2 = k_2 a = \frac{2\pi\nu}{c_2} a; \quad \text{și } x_3 = k_3 a = \frac{2\pi\nu}{c_3} a$	
$c_1 = \sqrt{\frac{E(1-\sigma)}{\rho_1(1+\sigma)(1-2\sigma)}} \quad c_2 = \sqrt{\frac{E}{2\rho_1(1+\sigma)}} \quad c_3 = 343 \frac{m}{s}$	

Simulation parameters for acoustic scattering by spherical scattering objects composed of two layers of materials with different elastic properties

In the performed simulations, the value of the integer n was truncated to 0, 1 and 2.

The conditions, conditionalities and simulation parameters are presented below.

$p_s = P_0 \sum_{n=0}^{\infty} c_n P_n(\cos\theta) [j_n(k_3 r) - i n_n(k_3 r)] e^{-i\omega t}$	
$c_0 = -P_0(-i) \sin \eta_0 e^{i\eta_0}$	
$\tan \eta_0 = \tan \delta_0(x_3) \frac{[\tan \Phi_0 + \tan \alpha_0(x_3)]}{\tan \Phi_0 + \tan \beta_0(x_3)}$	$\delta_0(x_3) = \tan^{-1} \left[-\frac{j_0(x_3)}{n_0(x_3)} \right]$
	$\alpha_0(x_3) = \tan^{-1} \left[-\frac{x_3 j'_0(x_3)}{j_0(x_3)} \right]$ $= \tan^{-1} \left[\frac{x_3 j_1(x_3)}{j_0(x_3)} \right]$
	$\beta_0(x_3) = \tan^{-1} \left[-\frac{x_3 n'_0(x_3)}{n_0(x_3)} \right]$ $= \tan^{-1} \left[\frac{x_3 n_1(x_3)}{n_0(x_3)} \right]$
$\tan \Phi_0 = -\frac{\rho_3}{\rho_1} \tan \zeta_0(x_1, \sigma)$	
$\zeta_0(x_1, \sigma) = \tan^{-1} \left[-\frac{x_2^2 \frac{x_1 j'_0(x_1)}{x_1 j'_0(x_1) - j_0(x_1)}}{2 \frac{\sigma}{1-2\sigma} \frac{x_1^2 [j_0(x_1) - j''_0(x_1)]}{x_1 j'_0(x_1) - j_0(x_1)}} \right]$	
$j''_0(x) = \frac{1}{4} [j_{-2}(x) - 2j_0(x) + j_2(x)] = \frac{1}{4} [(-1)^2 j_2(x) - 2j_0(x) + j_2(x)] = \frac{1}{2} [j_2(x) - j_0(x)]$	
$\text{unde } x_1 = k_1 a = \frac{2\pi\nu}{c_1} a; \quad x_2 = k_2 a = \frac{2\pi\nu}{c_2} a; \quad \text{și } x_3 = k_3 a = \frac{2\pi\nu}{c_3} a$	
$c_1 = \sqrt{\frac{E(1-\sigma)}{\rho_1(1+\sigma)(1-2\sigma)}} \quad c_2 = \sqrt{\frac{E}{2\rho_1(1+\sigma)}} \quad c_3 = 343 \frac{m}{s}$	

$c_1 = 3P_0 \sin \eta_1 e^{i\eta_1}$

$\tan \eta_1 = \tan \delta_1(x_3) \frac{[\tan \Phi_1 + \tan \alpha_1(x_3)]}{\tan \Phi_1 + \tan \beta_1(x_3)}$	$\delta_1(x_3) = \tan^{-1} \left[-\frac{j_1(x_3)}{n_1(x_3)} \right]$
	$\alpha_1(x_3) = \tan^{-1} \left[-\frac{x_3 j_1'(x_3)}{j_1(x_3)} \right]$
	$\beta_1(x_3) = \tan^{-1} \left[-\frac{x_3 n_1'(x_3)}{n_1(x_3)} \right]$
$\tan \Phi_1 = -\frac{\rho_3}{\rho_1} \tan \zeta_1(x_1, \sigma)$ $\zeta_1(x_1, \sigma) = \tan^{-1} \left[-\frac{x_2^2 \frac{x_1 j_1'(x_1)}{x_1 j_1'(x_1) - j_1(x_1)} - \frac{4j_1(x_2)}{x_2^2 j_2''(x_2)}}{2 \frac{x_1^2 \left[\frac{\sigma}{1-2\sigma} j_1(x_1) - j_1''(x_1) \right]}{x_1 j_1'(x_1) - j_1(x_1)} - \frac{4[j_1(x_2) - x_2 j_1'(x_2)]}{x_2^2 j_1''(x_2)}} \right]$ <p>unde $x_1 = k_1 a = \frac{2\pi\nu}{c_1} a$; $x_2 = k_2 a = \frac{2\pi\nu}{c_2} a$; și $x_3 = k_3 a = \frac{2\pi\nu}{c_3} a$</p> $c_1 = \sqrt{\frac{E(1-\sigma)}{\rho_1(1+\sigma)(1-2\sigma)}} \quad c_2 = \sqrt{\frac{E}{2\rho_1(1+\sigma)}} \quad c_3 = 343 \frac{m}{s}$	
$c_2 = 5P_0 i \sin \eta_2 e^{i\eta_2}$	
$\tan \eta_2 = \tan \delta_2(x_3) \frac{[\tan \Phi_2 + \tan \alpha_2(x_3)]}{\tan \Phi_2 + \tan \beta_2(x_3)}$	$\delta_2(x) = \tan^{-1} \left[-\frac{j_2(x_3)}{n_2(x_3)} \right]$
	$\alpha_2(x_3) = \tan^{-1} \left[-\frac{x_3 j_2'(x_3)}{j_2(x_3)} \right]$
	$\beta_2(x_3) = \tan^{-1} \left[-\frac{x_3 n_2'(x_3)}{n_2(x_3)} \right]$
$\tan \Phi_2 = -\frac{\rho_3}{\rho_1} \tan \zeta_2(x_1, \sigma)$ $\zeta_2(x_1, \sigma) = \tan^{-1} \left[-\frac{x_2^2 \frac{x_1 j_2'(x_1)}{x_1 j_2'(x_1) - j_2(x_1)} - \frac{12j_2(x_2)}{4j_2(x_2) + x_2^2 j_2''(x_2)}}{2 \frac{x_1^2 \left[\frac{\sigma}{1-2\sigma} j_2(x_1) - j_2''(x_1) \right]}{x_1 j_2'(x_1) - j_2(x_1)} - \frac{12[j_2(x_2) - x_2 j_2'(x_2)]}{4j_2(x_2) + x_2^2 j_2''(x_2)}} \right]$ <p>Unde $x_1 = k_1 a = \frac{2\pi\nu}{c_1} a$; $x_2 = k_2 a = \frac{2\pi\nu}{c_2} a$; și $x_3 = k_3 a = \frac{2\pi\nu}{c_3} a$</p> $c_1 = \sqrt{\frac{E(1-\sigma)}{\rho_1(1+\sigma)(1-2\sigma)}} \quad c_2 = \sqrt{\frac{E}{2\rho_1(1+\sigma)}} \quad c_3 = 343 \frac{m}{s}$	

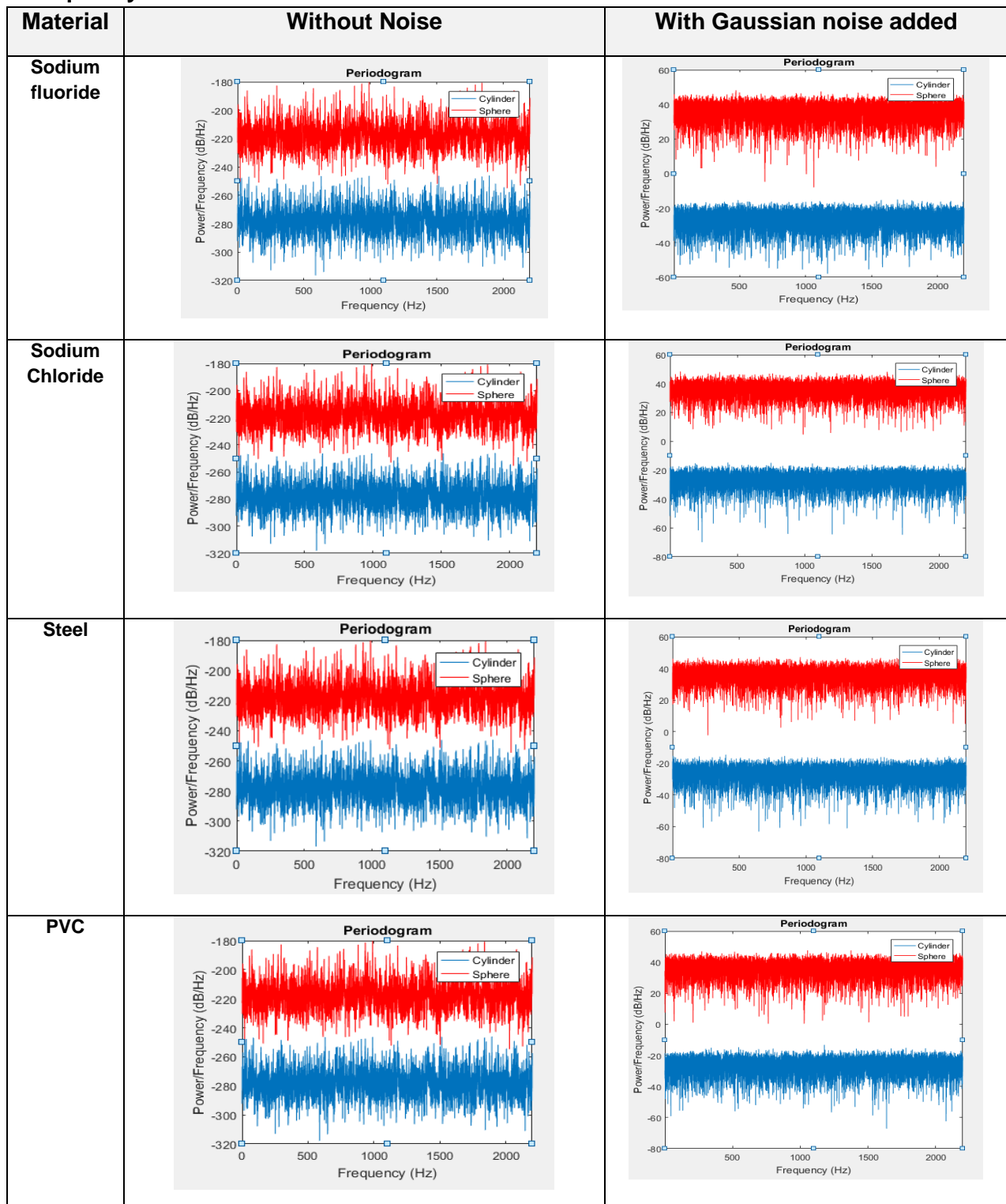
The analyzed materials were: sodium fluoride, sodium chloride, steel, PVC.

ro1=2560; ρ_1 sodium fluoride density [kg/m³]
 ro1=2170; ρ_1 sodium chloride density [kg/m³]
 ro1=7800; ρ_1 steel density [kg/m³]
 ro1=1380; ρ_1 PVC density [kg/m³]

E=79.01*(10⁹); Young's modulus for sodium fluoride
 E=39.98*(10⁹); Young's modulus for sodium chloride
 E=200*(10⁹); Young's modulus for steel
 E=2.48*(10⁹); Young's modulus for PVC
 sigma=0.35; Poisson's ratio

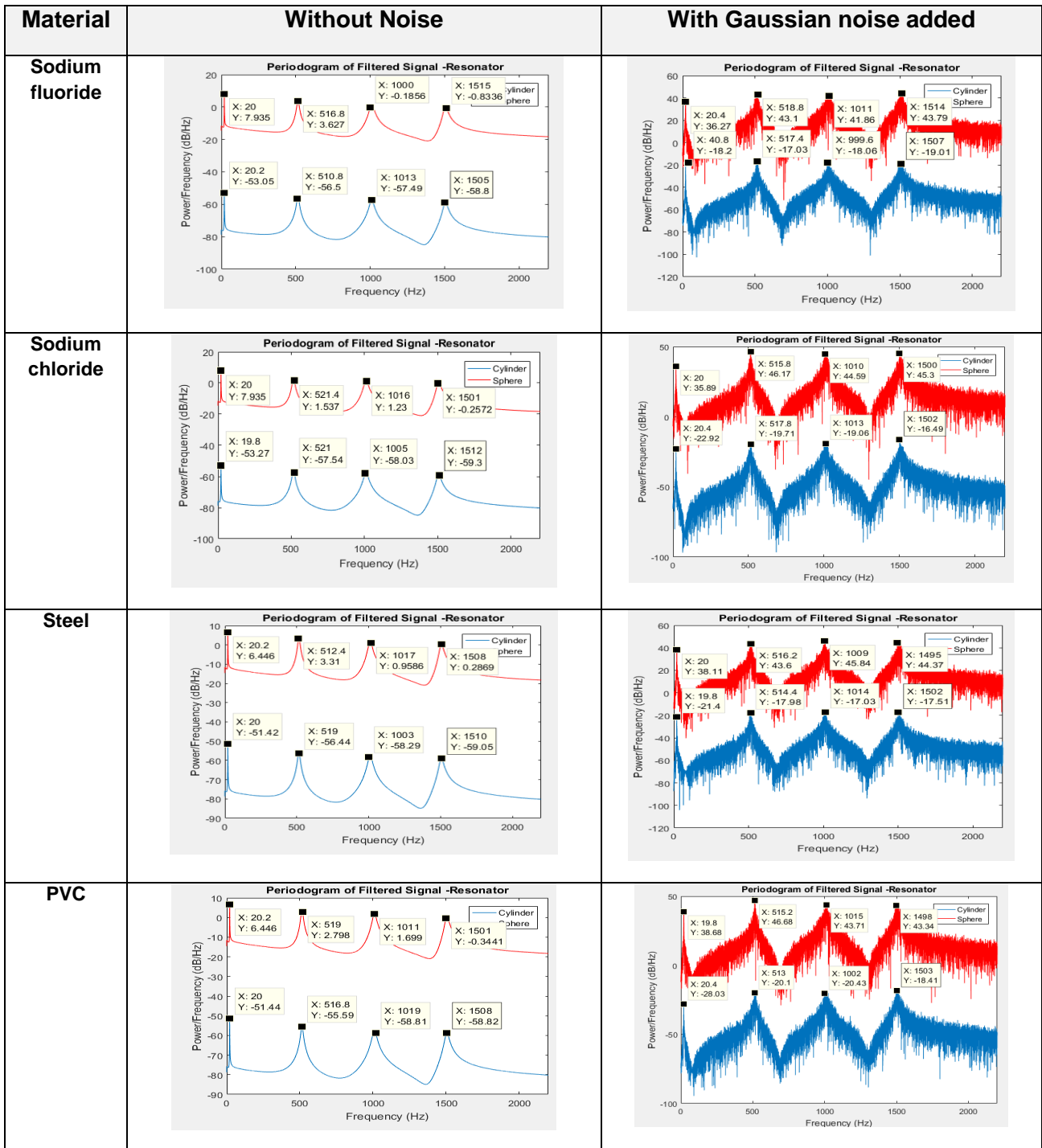
Periodograms (raw signal spectrum) for two-layer geometry (air-material) for solid and elastic objects of cylindrical and spherical shape

Frequency band 20-2000 Hz



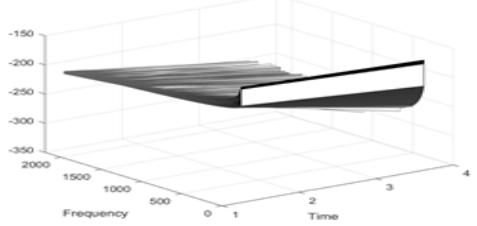
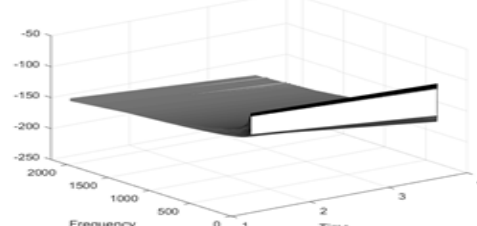
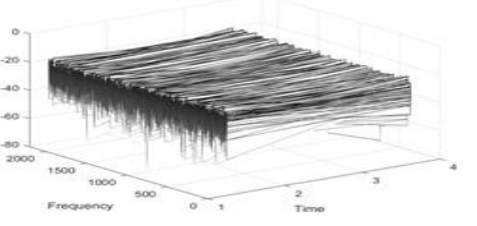
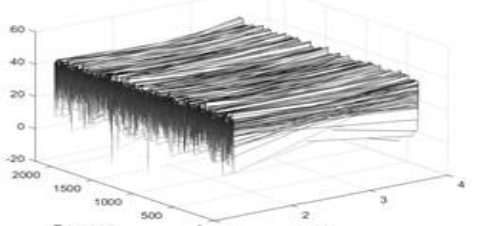
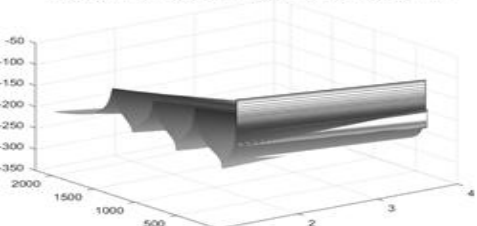
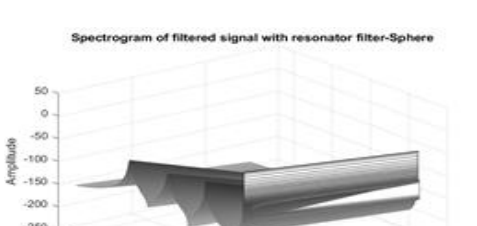
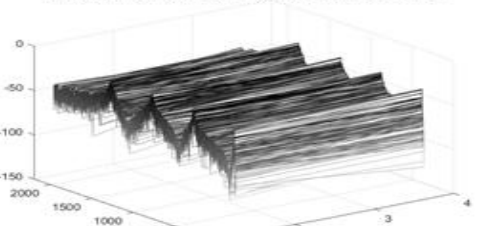
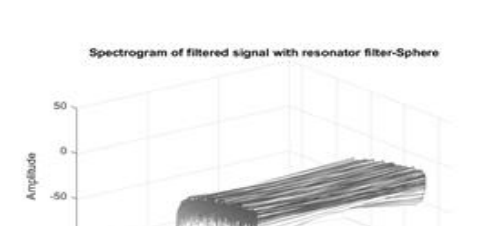
Periodograms for two-layer geometry (air-material) in case of solid and elastic objects of cylindrical and spherical shape - HR Resonator Filter

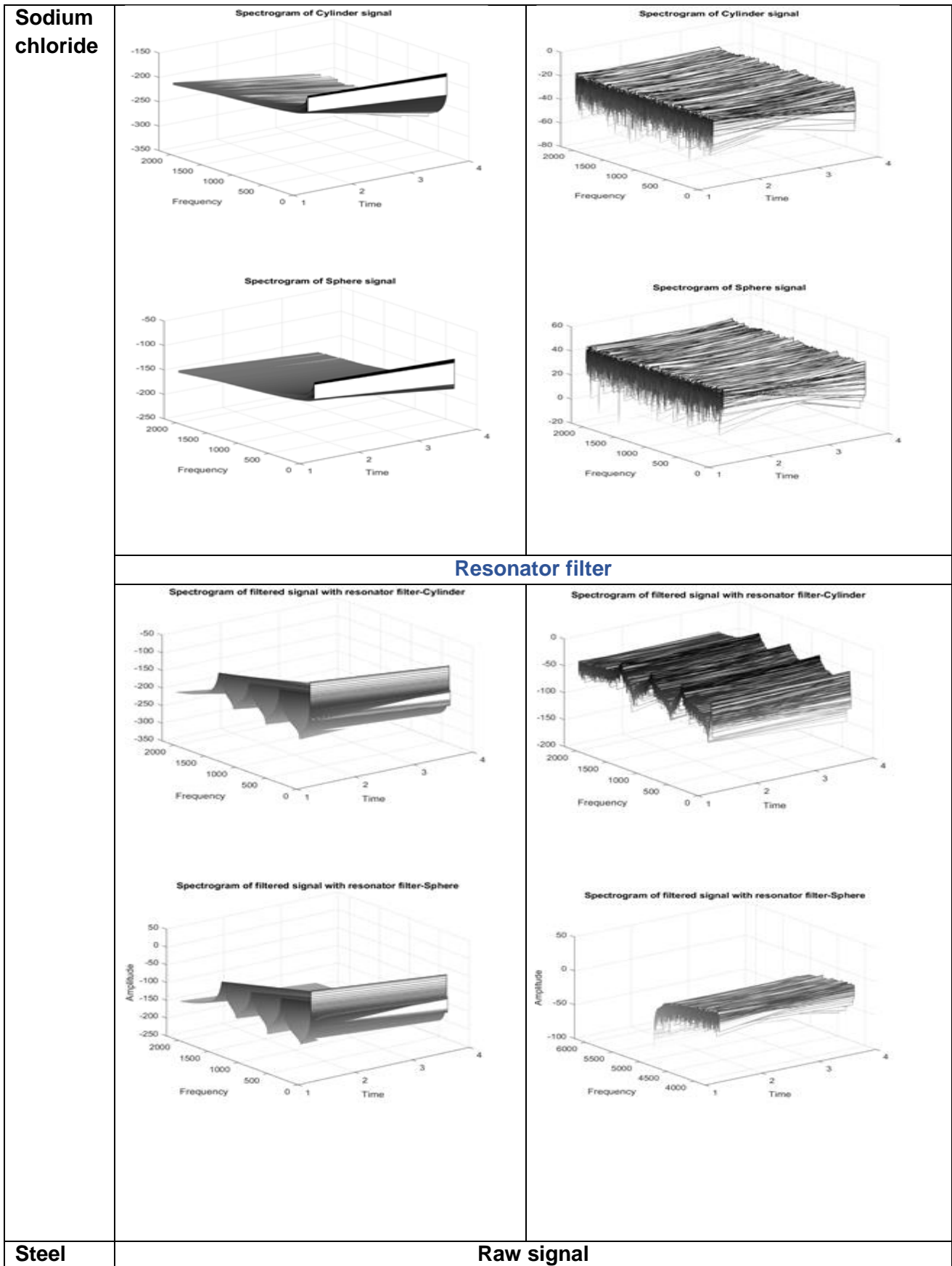
Frequency band 20-2000 Hz

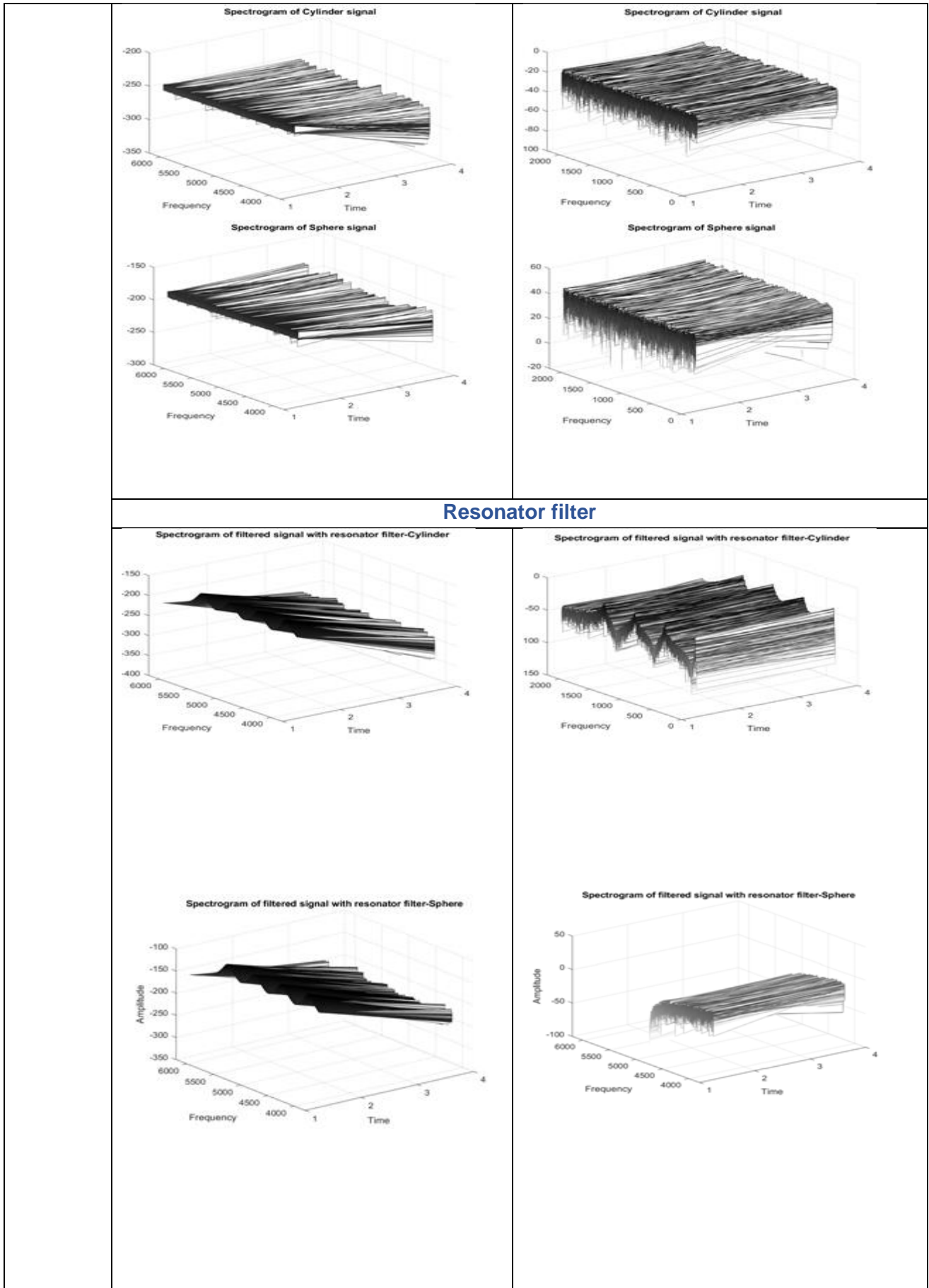


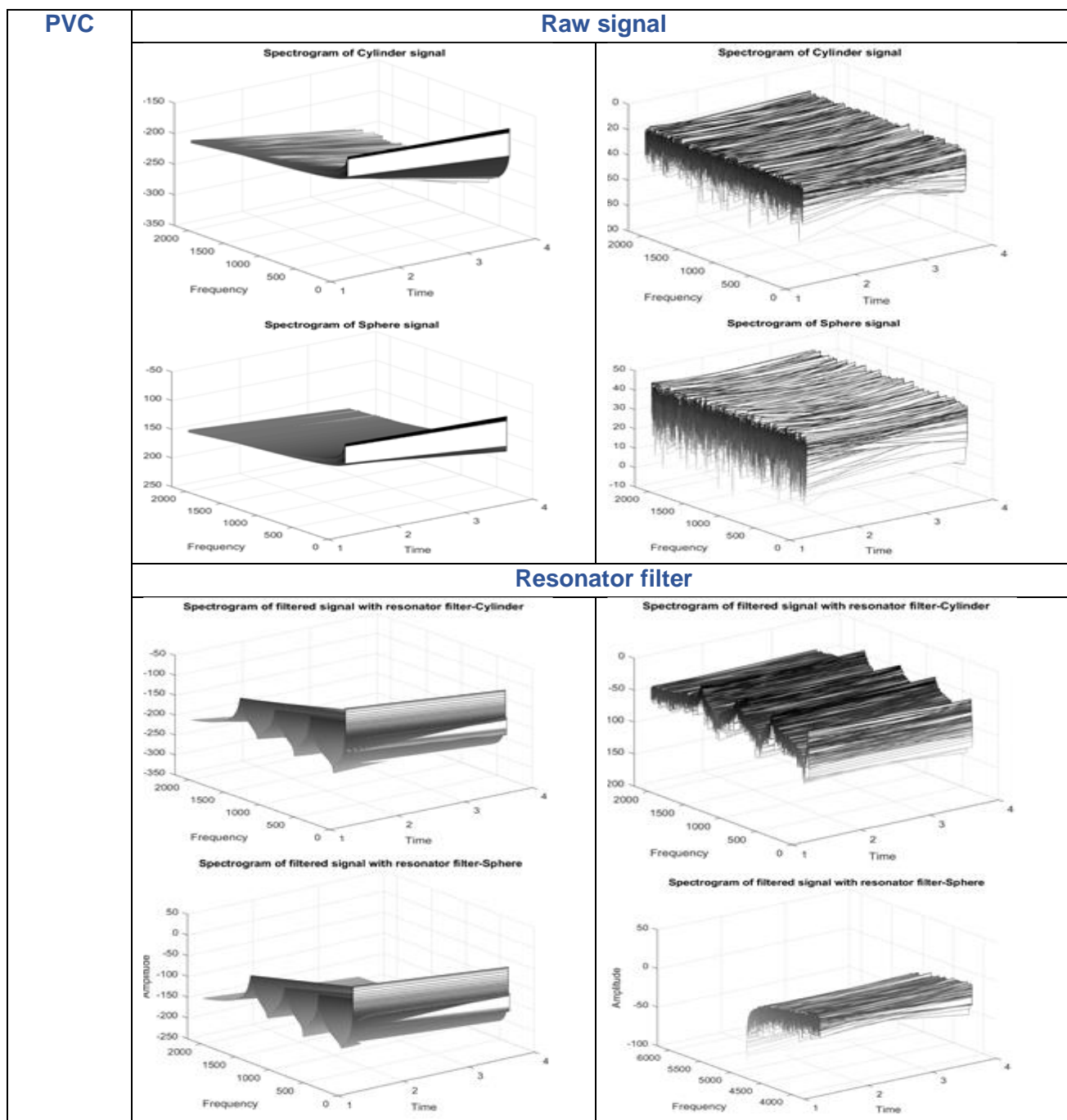
3D spectrograms for two-layer geometry (air-material) for solid and elastic objects of cylindrical and spherical shape. The results provided by the resonator filter are presented.

Frequency band 20-2000 Hz

Material	Without Noise	With Gaussian noise added
Sodium fluoride	Raw signal	
	<p style="text-align: center;">Spectrogram of Cylinder signal</p>  <p style="text-align: center;">Spectrogram of Sphere signal</p> 	<p style="text-align: center;">Spectrogram of Cylinder signal</p>  <p style="text-align: center;">Spectrogram of Sphere signal</p> 
Resonator filter		
	<p style="text-align: center;">Spectrogram of filtered signal with resonator filter-Cylinder</p>  <p style="text-align: center;">Spectrogram of filtered signal with resonator filter-Sphere</p> 	<p style="text-align: center;">Spectrogram of filtered signal with resonator filter-Cylinder</p>  <p style="text-align: center;">Spectrogram of filtered signal with resonator filter-Sphere</p> 
	Raw signal	







Due to the simulation data presented for the investigation of the acoustic field scattered by elastic objects when considering the double layer approach (air-material) at the border of the diffusing object, it may be concluded that:

- There are no differences between the results provided in a local approach (distance between the transmitter and the investigated system of 5 cm) and the distance/far approach (distance between the transmitter and the investigated system of 100 cm). In our simulation, a clear separation of the scattered signals of cylindrical and spherical elastic objects was highlighted for all the investigated materials.
- It should be noted from the periodograms that, despite the fact that the shape of the signal is changed by backpropagation, the only notable change was the modification

of the power / frequency ratio. This rate grows as the distance between the transmitter / broadcast system increases.

- The highest peaks / response peaks of the scattered signal are around the following frequencies, 20 Hz, 500 Hz, 1000 Hz and 1500 Hz. There are very small variations for different experimental conditions (less than 1%).

The spectrograms clearly indicate the absorption bands for each resonant frequency provided by the resonance filter.

Chapter 4 Acoustic backscattering simulations by targets with complex geometric features and on multiple targets

4.1. Analysis of acoustic backscattering by non-convex kite-shape objects in the low frequency domain

This section presents the results of the simulation for acoustic scattering problems for transparent / easily penetrating acoustic obstacles, acoustically impenetrable / rigid obstacles to the propagation of some acoustic and absorbing obstacles due to the scattering of plane acoustic waves by non-convex kite-shape objects. Simulation experiments on acoustic scattering were performed in several configurations (with the same obstacles, but with varying sizes and orientations), using equations that allow the construction of scattering objects with different characteristics. Furthermore, the results associated with the acoustic scattering in the approximate distant fields and the values of the associated acoustic cross section (ACS) of the scattering configuration on the analysis directions are also presented. The experimental results are obtained in so called bistatic (i.e., the receiver is placed somewhere else than the transmitter) or single parameter estimation

For our simulation purposes, three dimensions of obstacles with a non-convex kite-shape cross-section acoustic section are used as follows:

- A. $x(t) = (\cos t + 0.65 \cos 2t, 1.5 \sin t) \quad 0 \leq t \leq 2\pi$
- B. $x(t) = (\cos t + 0.75 \cos 2t, 1.5 \sin t) \quad 0 \leq t \leq 2\pi$
- C. $x(t) = (\cos t + 0.75 \cos 2t, 2 \sin t) \quad 0 \leq t \leq 2\pi$

Additionally, two wavelengths $k = 12,5664 (4\pi)$ and $6,2832 (2\pi)$ are used. The results of the simulation for the intensity of the scattered field behind the obstacles from a plane wave propagating in the x direction are presented.

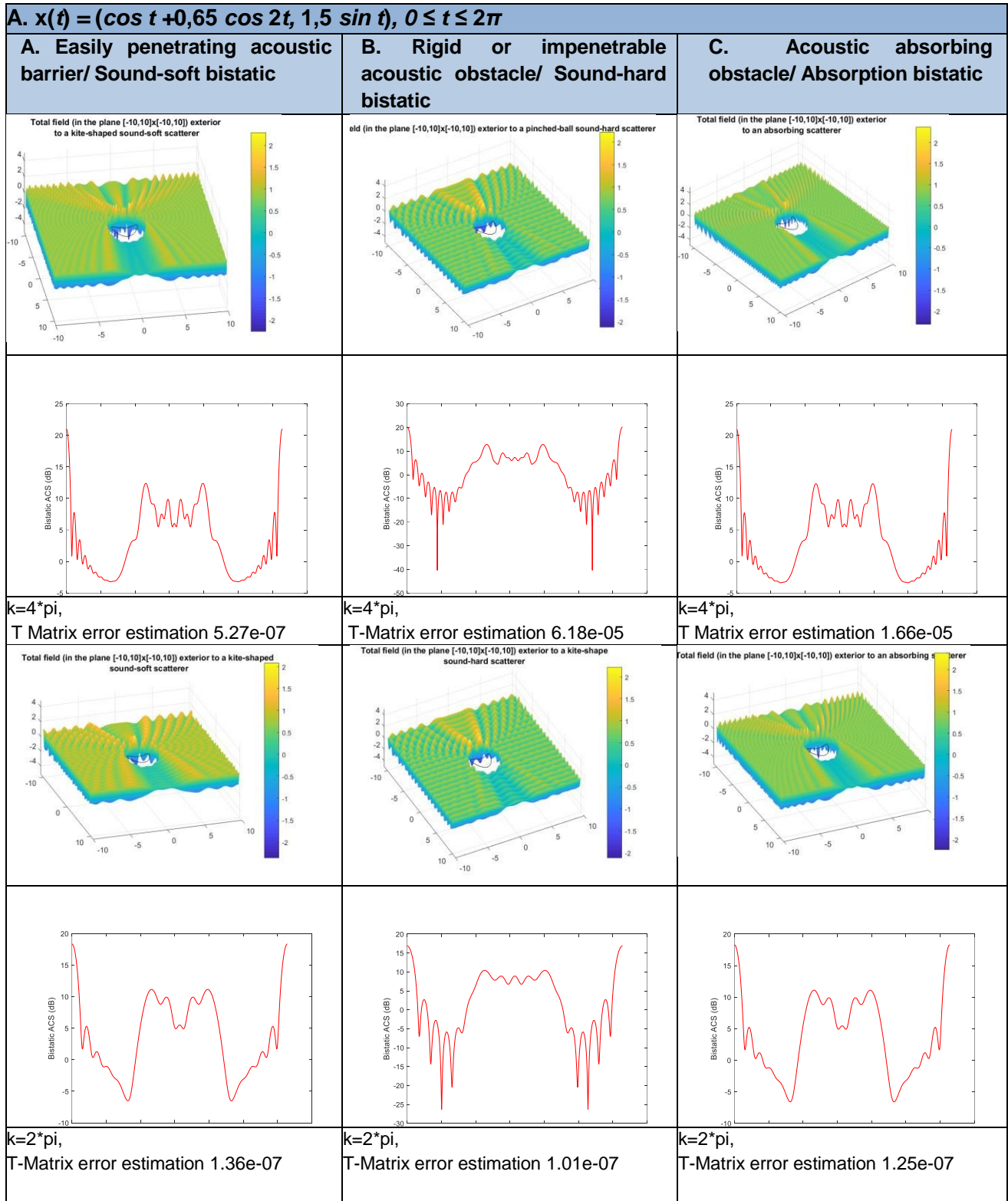


Fig. 4.1. Visualization of the scattered field and detection of the region without radiation (shadows) behind the deltoid obstacle $x(t) = (\cos t + 0.65 \cos 2t, 1.5 \sin t)$ (lines 1 and 3) and the variation of the acoustic cross section (ACS) for the deltoid obstacle calculated using the T matrix (lines 2 and 4) and the declared parameters. The simulation uses bistatic detection.

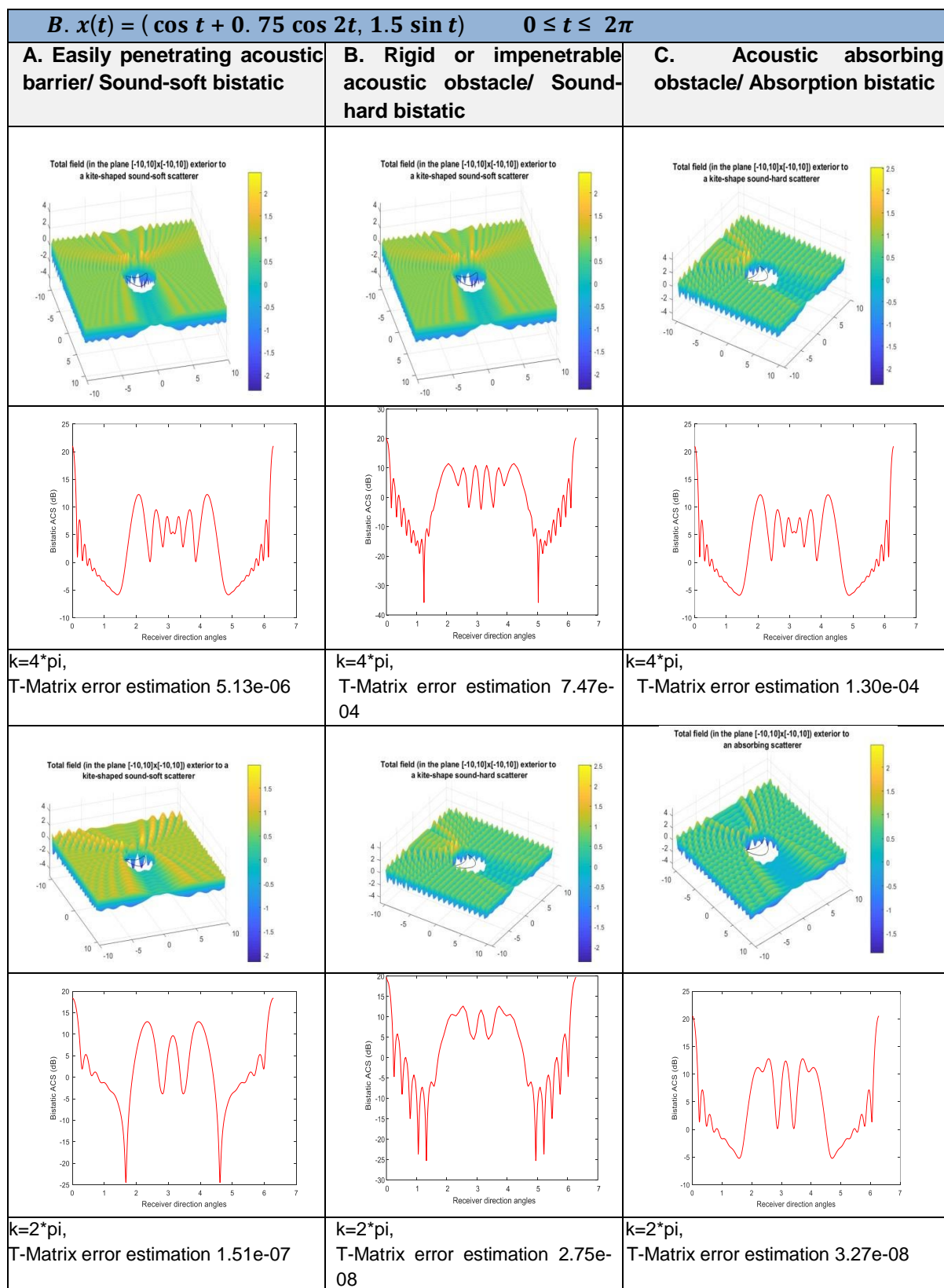


Fig. 4.2. Visualization of the scattered field and detection of the region without radiation (shadows) behind the kite-shape obstacle $x(t) = (\cos t + 0.75 \cos 2t, 1.5 \sin t)$ (lines 1 and 3) and the variation of the acoustic cross section (ACS) for the deltoid obstacle calculated

using the T matrix (lines 2 and 4) and the declared parameters. The simulation uses bistatic detection.

C. $x(t) = (\cos t + 0.75 \cos 2t, 2 \sin t)$ $0 \leq t \leq 2\pi$		
A. Easily penetrating acoustic barrier/ Sound-soft bistatic	B. Rigid or impenetrable acoustic obstacle/ Sound-hard bistatic	C. Acoustic absorbing obstacle/ Absorption bistatic
<p>Total field (in the plane [-10,10]x[-10,10]) exterior to a kite-shaped sound-soft scatterer</p>	<p>Total field (in the plane [-10,10]x[-10,10]) exterior to a kite-shaped sound-hard scatterer</p>	<p>Total field (in the plane [-10,10]x[-10,10]) exterior to an absorbing scatterer</p>
<p>Bistatic ACS (dB)</p> <p>Receiver direction angles</p>	<p>Bistatic ACS (dB)</p> <p>Receiver direction angles</p>	<p>Bistatic ACS (dB)</p> <p>Receiver direction angles</p>
$k=4*\pi$, T-Matrix error estimation 6.25e-05	$k=4*\pi$, T-Matrix error estimation 1.82e-03	$k=4*\pi$, T-Matrix error estimation 4.03e-04
<p>Total field (in the plane [-10,10]x[-10,10]) exterior to a kite-shaped sound-soft scatterer</p>	<p>Total field (in the plane [-10,10]x[-10,10]) exterior to a kite-shaped sound-hard scatterer</p>	<p>Total field (in the plane [-10,10]x[-10,10]) exterior to an absorbing scatterer</p>
<p>Bistatic ACS (dB)</p> <p>Receiver direction angles</p>	<p>Bistatic ACS (dB)</p> <p>Receiver direction angles</p>	<p>Bistatic ACS (dB)</p> <p>Receiver direction angles</p>
$k=2*\pi$, T-Matrix error estimation 3.55e-08	$K=2*\pi$, T-Matrix error estimation 2.75e-08	$K=2*\pi$, T-Matrix error estimation 3.27e-08

Fig. 4.3. Visualization of the scattered field and detection of the region without radiation (shadows) behind the kite-shape obstacle $x(t) = (\cos t + 0.75 \cos 2t, 2 \sin t)$ (lines 1 and 3) and the variation of the acoustic cross section (ACS) for the deltoid obstacle calculated using the T matrix (lines 2 and 4) and the declared parameters. The simulation uses bistatic detection.

The accuracy of the T-matrix estimation is between $error = 1.82e-03$ for a sound-hard bistatic object of the form $x(t) = (\cos t + 0.75 \cos 2t, 2 \sin t)$ and $k = 2\pi$ up to $error = 2.75e-08$ for a rigid or impenetrable acoustic object of the form $x(t) = (\cos t + 0.75 \cos 2t, 1.5 \sin t)$ and $k = 2\pi$. A better estimation of the acoustic scattering is observed for acoustic waves with higher wavelengths (lower frequencies). Observe, however, that a good estimate of the T-matrix error can be obtained in the far field induced by an acoustic wave with a shorter wavelength (higher frequency). One could also note that there are no clearly defined behaviors regarding the variation of the bistatic cross-sectional acoustic section in the case of easily penetrated acoustically/ sound-soft bistatic and absorbent obstacles/ absorption bistatic. This finding is expectable because both cases involve an amount of incident acoustic energy absorbed in the surface layers of the obstacle. There was also a greater accuracy in estimating ACS, by increasing the number of "peaks" in the case of rigid or impenetrable acoustic obstacle, although it is observed that the secondary scattering is well represented likewise. This outcome is based on the fact that all the energy of the incident acoustic field is "turned" by the object into the far acoustic field and is distributed between the central lobe and the secondary lobes.

The results of the simulations indicate a higher accuracy of the T-matrix model for the cases of the far field generated by acoustic waves with lower wavelengths.

4.2. Simulation of backscattering of acoustic waves by multiple targets - an optimization problem

The aims of this research are to evaluate the accuracy of target location using the values of phase and amplitude provided by the K matrix, and the amplitude of scattered signals provided by the MUSIC pseudospectrum in the far-field condition. To detect and locate a finite number of small scattering targets relative to the incident wavelength, we used the Multiple Signal Classification (MUSIC) algorithm that analyses a multitude of scatterers placed in specific geometries [71, 80, 81, 139-142]. By studying the problem of backscattering of sound waves we aimed to locate an inhomogeneity in the environment, which is seen as a disruptor, using the knowledge of the waves scattered by it.

MUSIC operates based on the assumption that the far field patterns of point sources are almost orthogonal to the noise subspace of the far field operator or so called multistatic matrix data K and both the Born model of approximating a distorted acoustic wave DWBA (i.e. the amplitude of the scattered wave is much smaller than the amplitude of the incident wave) and the more general scattering models that consider multiple scattering between targets, i.e. the Foldy-Lax (FL) formulation of the multiple scatter pattern.

The results of this simulation study are based on the determination of the position of the scattering objects, starting from measurements of the *magnitude and phase of the scattered signals reconstructed by using the multistatic matrix data K*, in the approximation of

the far field condition. K is obtained for a collection of M targets and an active array of N transceivers. The targets are placed in a propagation medium with known properties. The MUSIC algorithm does not need to know the type of targets that need to be detected nor does it need to determine the properties of these targets. In this study, we extend the scope to the low frequency range, but the condition of homogeneity of the presumed known propagation medium remains unchanged. We are focusing on the data collected at 5, 10, 50 and 100 Hz (or normalized wavelengths of 1, 0.5, 0.1, and 0.05) in order to develop a new scanning technology applicable in a nondivest and noncontact condition, so that the condition that the targets are much smaller than the wavelength is met. The position of the point targets is reconstructed and placed in a homogeneous propagation medium, within the limits of the FL and DWBA approximations [157-159].

The optimization, which is based on locating targets placed at short distances from each other, is yet another challenge in an environment affected by noise. The data collected by the sensors are inaccurate and the reconstructed signals show important differences compared to the data provided by the propagation in environments unaffected by noise. Extreme noise values are used, i.e. maximum value $P = 0.09$ and minimum value $P = 0.0009$ to investigate and optimize the spatial distribution of targets in relation to the different values of wavelength and how noise affects the reconstruction process. A new aspect is addressed here: the investigation of the amplitude and phase distribution of the singular vectors obtained from the Singular Value Decomposition (SVD) of the matrix K in both approximations through the Fréchet distance measurement in order to quantify the distance between the amplitude and phase curves vs. the number of transceivers in both approximations. The proper scatterer detection is provided by these target geometries and set of parameters, which minimize the Fréchet distance and maximize the amplitude of the reconstructed signal. The block diagram of the proposed method is shown in Figure 4.4

An optimization problem for four forms of spatial distribution of targets was analyzed. Figure 4.5 describes the geometry of the transmitters (represented as squares) and of the targets (represented as circles). $N = 10$ transceivers in a coincident linear array are located at $(-20,0)$; $(-15,0)$; $(-10,0)$; $(-5,0)$ and $(-2,0)$. Targets are set as follows:

- Triangle configuration (T), $(0, -8)$, $(-1, -9)$, $(1, -9)$, $(-2, -10)$, $(0, -10)$, $(2, -10)$;
- Parallelogram configuration (P), $(-2, -8)$, $(0, -8)$, $(2, -8)$, $(0, -9)$, $(2, -9)$, $(4, -9)$;
- Diamond configuration (D), $(0, -6)$, $(-2, -8)$, $(0, -10)$, $(2, -8)$, $(0, -7)$, $(0, -9)$;
- Elliptic configuration (E), $(0, -8)$, $(-3, -9)$, $(3, -9)$, $(-3, -10)$, $(3, -10)$.

All positions are correlated with the λ wavelength values. The spatial separation of the targets in the chosen geometric configurations is of the following size: λ , $\sqrt{2}\lambda$ and 2λ . The scattering coefficient or scattering power of the targets is $\tau = (1; 1.3; 1.6; 1.6; 1.3; 1)$.

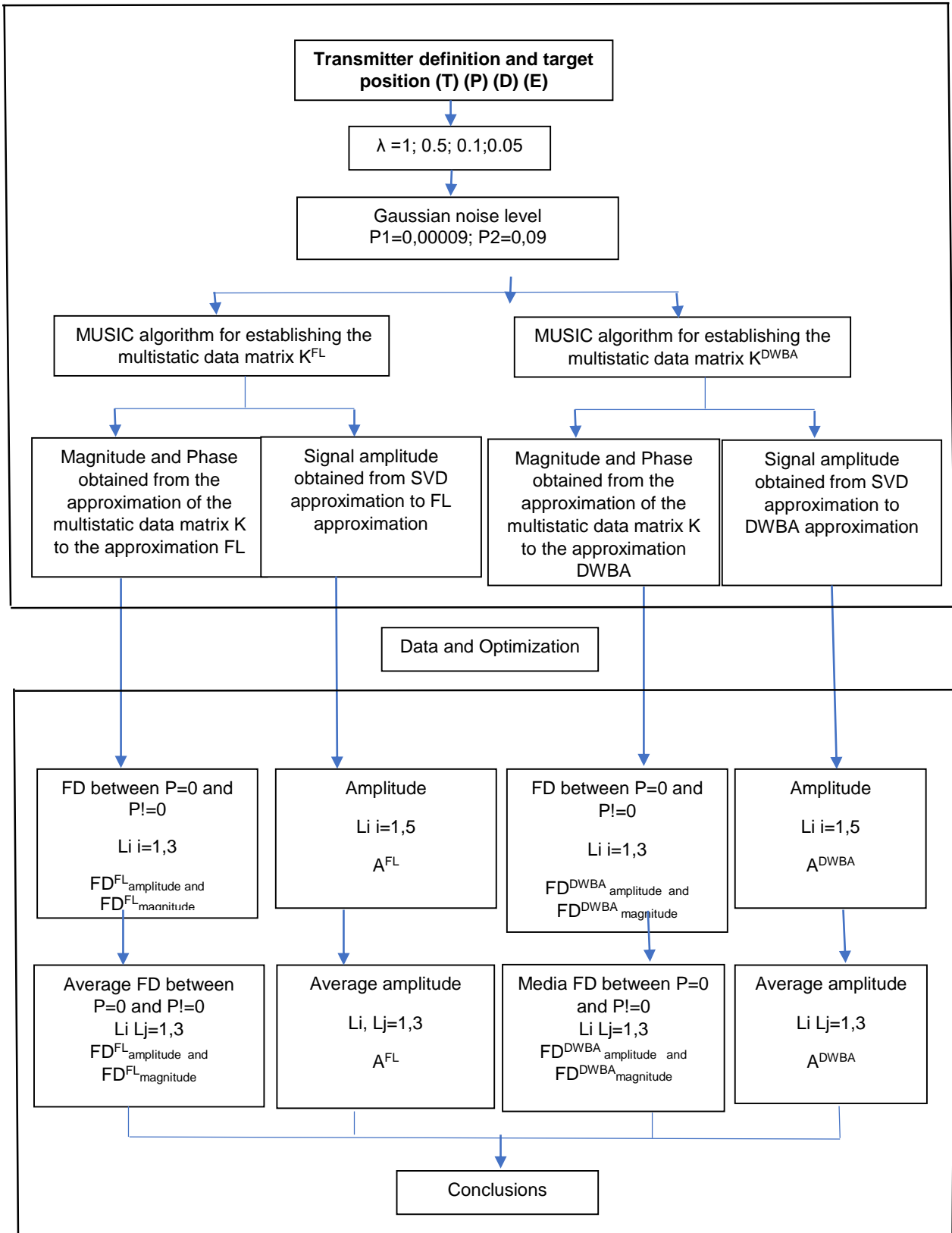


Figure 4.4 - Block diagram

Examples of simulation of propagation space and reconstruction results, for DWBA and FL approximation, are shown in Figures 4.7 - 4.10, in case the targets have a triangular

spatial location and for all simulation parameters. In order to optimize the process, both the phase and amplitude distribution of the singular vectors obtained from SVD of matrix K in FL and DWBA methods are presented in Fig. 4.6. The problem applies to both noise-free and noise-affected data.

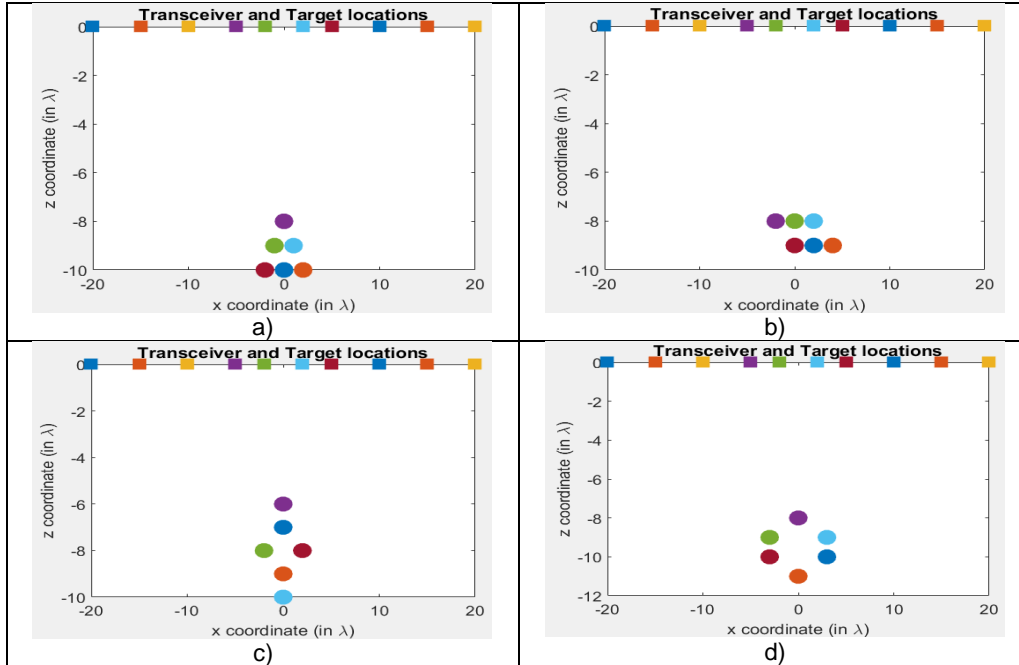


Figure 4.5. Problem setup: 10 transceivers (depicted as squares) and 6 targets (depicted as circles) are embedded in uniform background. Targets' spatial distributions are represented as a) Triangle (T); b) Parallelogram (P); c) Diamond (D), and d) Ellipse (E).

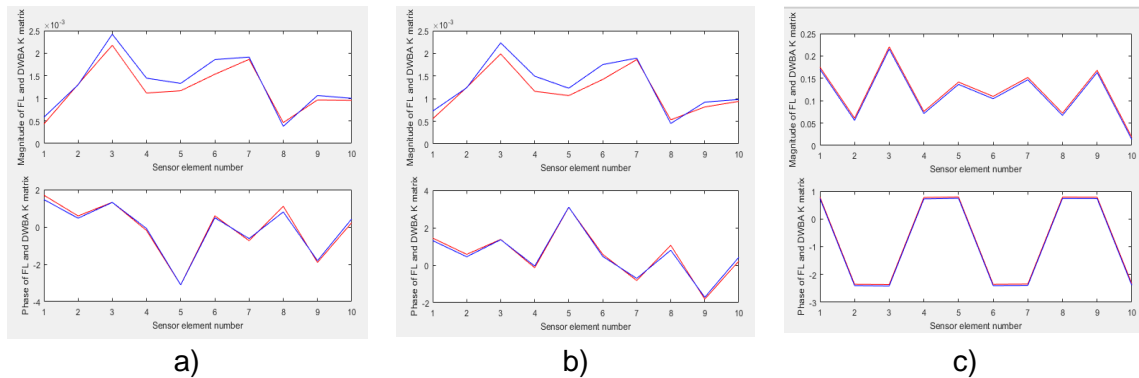


Figure 4.6. Curves of individual components: 'amplitude' (top) and 'phase' (bottom) provided by the left singular vectors obtained from SVD of the matrix K in FL approximation (blue) and DWBA approximation (red) vs. number $N = 10$ of array elements in triangle (T) geometry and for $\lambda = 1$. a) $P = 0$ (Noise-free); b) $P=0,00009$ (random noise); c) $P = 0,09$ (random noise).

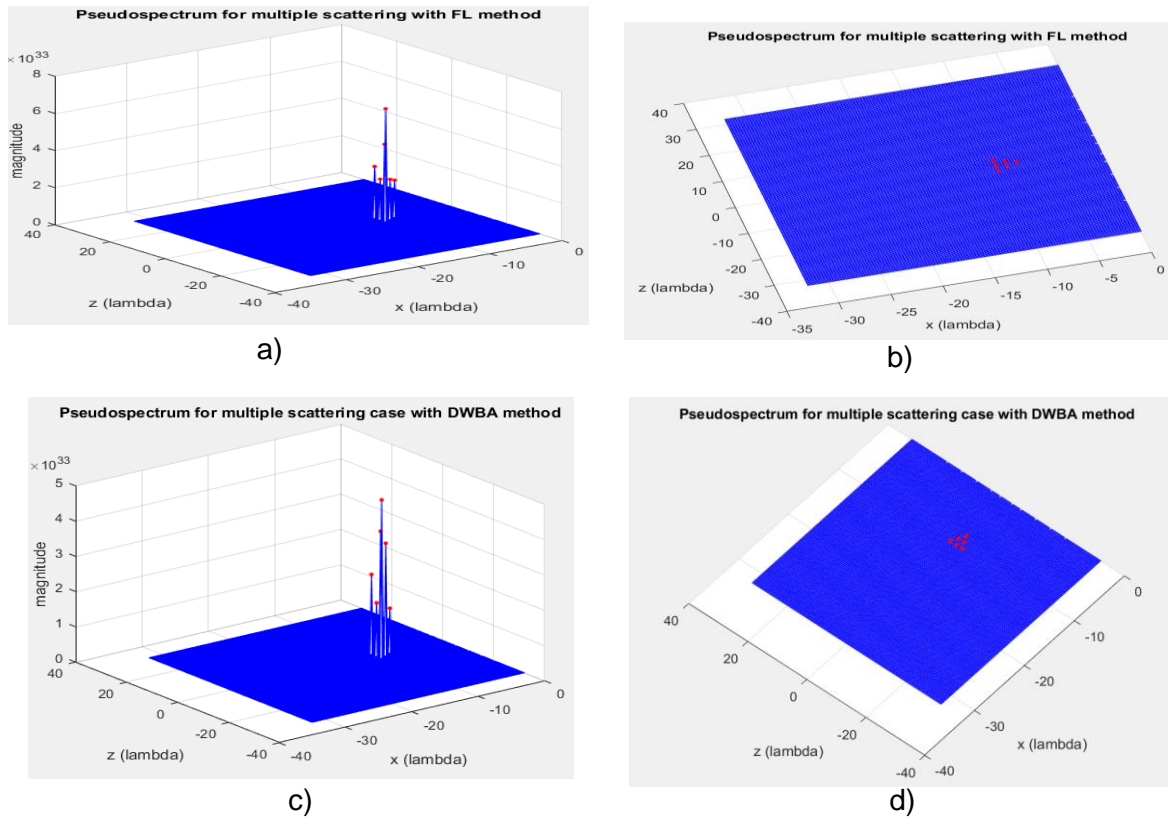
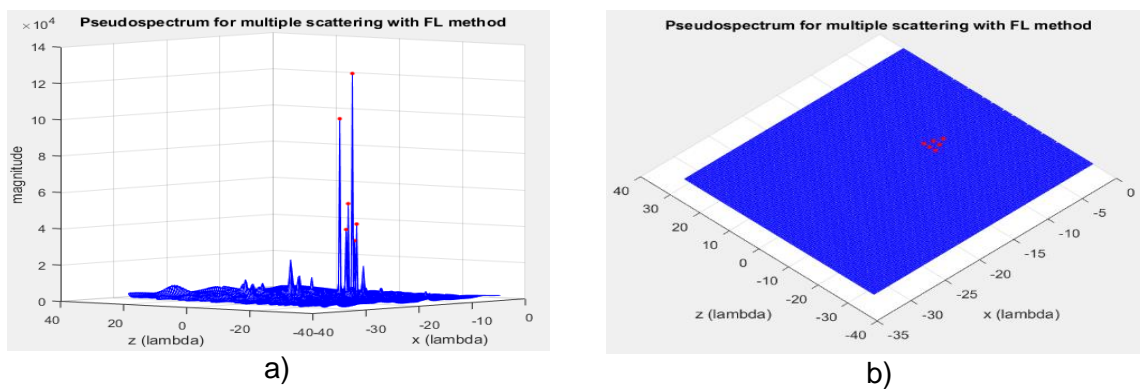


Figure 4.7 Exact location of targets obtained by reconstructing the scattered signal for 3D (left column) and 2D (right column) visualization, for $P=0$ (noise free), $\lambda = 1$, in triangle (T) geometry, in SVD approach. a) - b) pseudospectrum for multiple scattering in the FL approximation; c) - d) pseudospectrum for multiple scattering in the DWBA approximation.



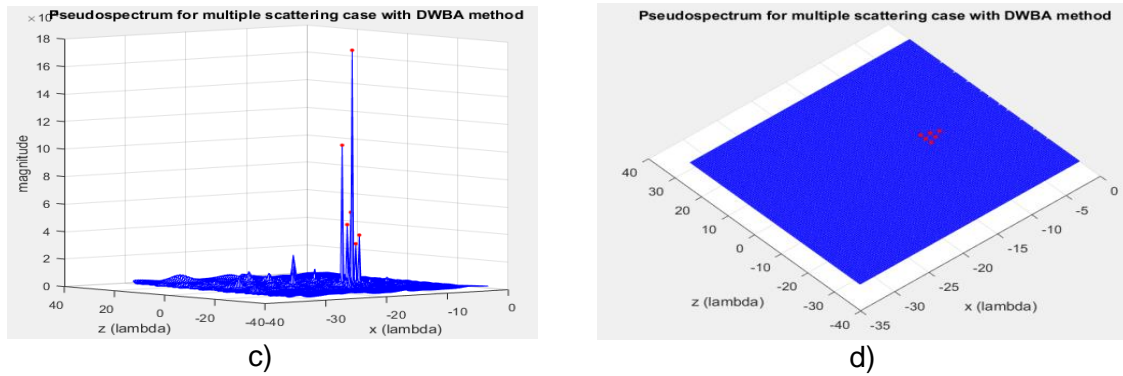


Figure 4.8 Exact target location obtained by reconstructing the scattered signal for 3D (left column) and 2D (right column) visualization, for $P = 0.00009$ (low value random noise), $\lambda = 1$, in triangle (T) geometry, in the SVD approach. a) - b) pseudospectrum for multiple scattering in the FL approximation; c) - d) pseudospectrum for multiple scattering in the DWBA approximation.

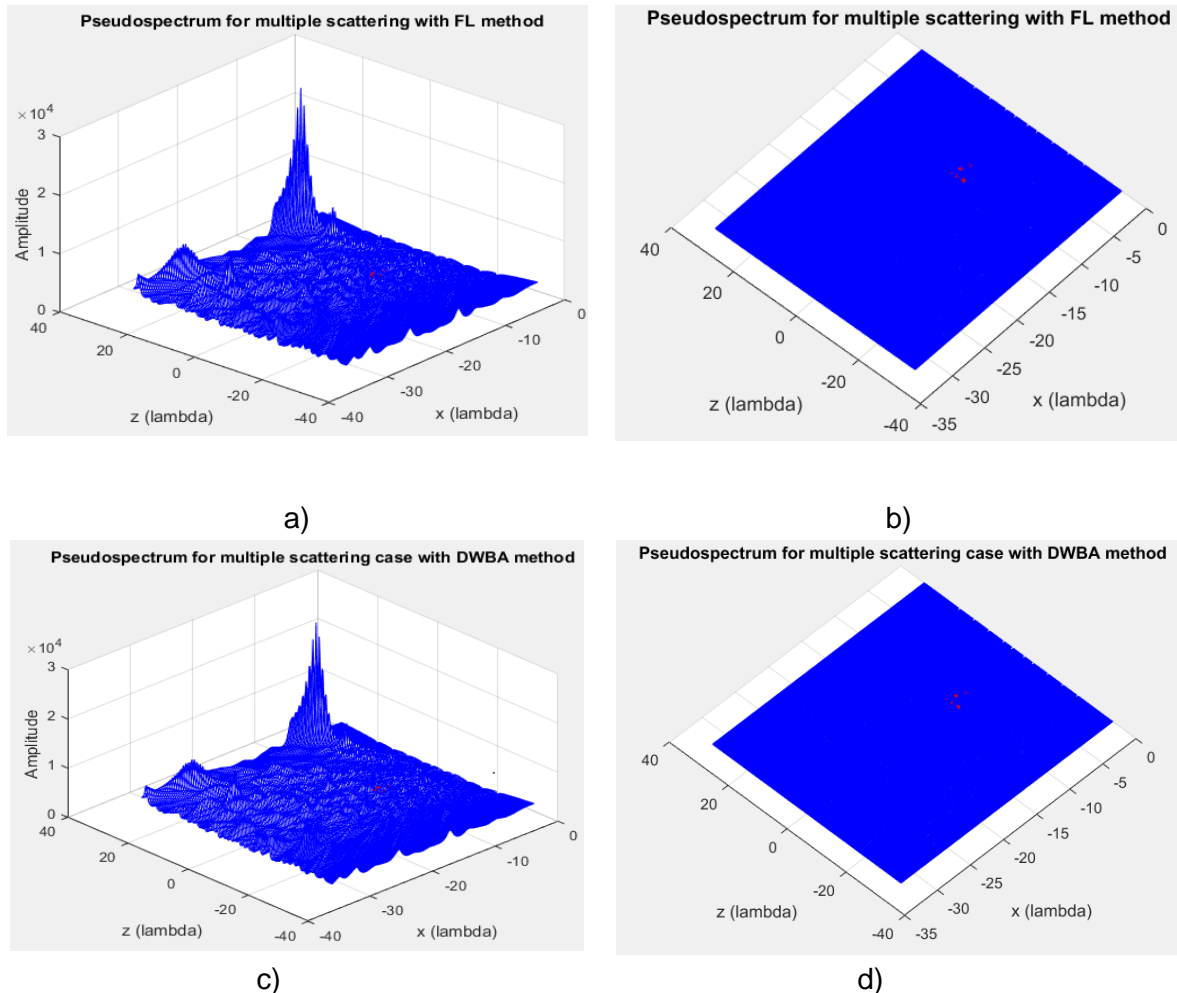


Figure 4.9 Exact target location obtained by reconstructing the scattered signal for 3D (left column) and 2D (right column) visualization, for $P = 0.09$ (high value random noise), $\lambda = 1$, in triangle (T) geometry, in the SVD approach. a) - b) pseudospectrum for multiple scattering in the FL approximation; c) - d) pseudospectrum for multiple scattering in the DWBA approximation.

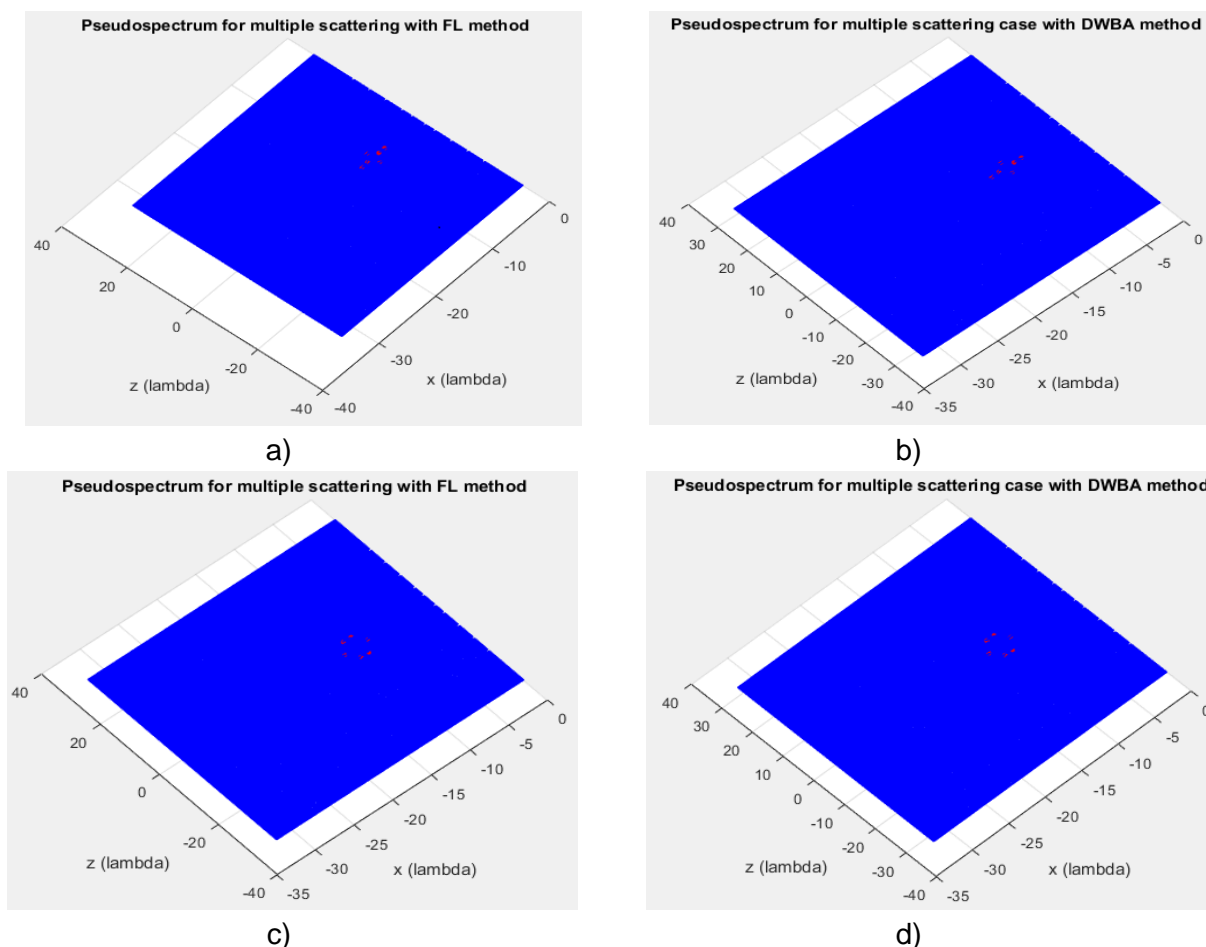


Figure 4.10. Detection of targets arranged in the diamond D (top line) and ellipse E (bottom line) geometries, in case for $P = 0.09$ (random noise), for FL and DWBA approximations..

Table 4.1. Fréchet distance (FD), the characteristic values "magnitude" and "phase" and the amplitude of the values of the scattered signals (A) obtained in the simulation experiments for 2D obstacles, extracted from the list Li ($i = 1: 6$).

Geometry	Noise Level (dB)	SNR (dB)	λ	Magnitude		Phase		Amplitude	
				FD^{FL}	FD^{DWBA}	FD^{FL}	FD^{DWBA}	A^{FL}	A^{DWBA}
(T)	0	-	1	-	-	-	-	3.18E+33	2.69E+33
		-	0.5	-	-	-	-	3.18E+33	2.69E+33
		-	0.1	-	-	-	-	1.43E+33	1.03E+33
		-	0.05	-	-	-	-	1.43E+33	1.03E+33
	0.00009	22.38	1	0.18E-3	0.20E-3	3.03582	3.12496	72073	63082
		22.38	0.5	0.18E-3	0.20E-3	3.03582	3.12496	72073	63082
		22.38	0.1	0.18E-3	0.20E-3	3.03582	3.12496	13173	12729
		22.38	0.05	0.18E-3	0.20E-3	3.03582	3.12496	13173	12729
	0.09	6.3	1	0.21688	0.21835	2.94609	3.00016	480	469
		6.3	0.5	0.21688	0.21835	2.94609	3.00016	480	469
		6.3	0.1	0.21688	0.21835	2.94609	3.00016	187	177

Sound scattering simulations on complex body systems

		6.3	0.05	0.21688	0.21835	2.94609	3.00016	187	177
(P)	0	-	1	-	-	-	-	5.72E+33	3.94E+33
		-	0.5	-	-	-	-	5.72E+33	3.94E+33
		-	0.1	-	-	-	-	1.56E+33	1.29E+33
		-	0.05	-	-	-	-	1.56E+33	1.29E+33
	0.00009	22.66	1	0.21E-3	0.00028	0.27809	0.28758	97896	91591
		22.66	0.5	0.21E-3	0.00028	0.27809	0.28758	97896	91591
		22.66	0.1	0.21E-3	0.00028	0.27809	0.28758	44955	43475
		22.66	0.05	0.21E-3	0.00028	0.27809	0.28758	44955	43475
	0.09	8.9	1	0.22223	0.22249	2.21685	2.27478	562	560
		8.9	0.5	0.22223	0.22249	2.21685	2.27478	562	560
		8.9	0.1	0.22223	0.22249	2.21685	2.27478	191	187
		8.9	0.05	0.22223	0.22249	2.21685	2.27478	191	187
(D)	0	-	1	-	-	-	-	3.61E+33	2.68E+33
		-	0.5	-	-	-	-	3.61E+33	2.68E+33
		-	0.1	-	-	-	-	8.76E+33	1.61E+33
		-	0.05	-	-	-	-	8.76E+33	1.61E+33
	0.00009	22.12	1	0.18E-3	0.00029	0.15783	0.21925	85708	77328
		22.12	0.5	0.18E-3	0.00029	0.15783	0.21925	85708	77328
		22.12	0.1	0.18E-3	0.00029	0.15783	0.21925	69885	61827
		22.12	0.05	0.18E-3	0.00029	0.15783	0.21925	69885	61827
	0.09	3.3	1	0.22100	0.22121	3.70183	3.70754	687	676
		3.3	0.5	0.22100	0.22121	3.70183	3.70754	687	676
		3.3	0.1	0.22100	0.22121	3.70183	3.70754	524	514
		3.3	0.05	0.22100	0.22121	3.70183	3.70754	524	514
(E)	0	-	1	-	-	-	-	4.79E+33	3.93E+33
		-	0.5	-	-	-	-	4.79E+33	3.93E+33
		-	0.1	-	-	-	-	9.35E+32	1.34E+33
		-	0.05	-	-	-	-	9.35E+32	1.34E+33
	0.00009	21.62	1	0.13E-3	0.0001	1.8960	0.2143	93064	75146
			0.5	0.13E-3	0.0001	1.8960	0.2143	93064	75146
			0.1	0.13E-3	0.0001	1.8960	0.2143	30912	24563
			0.05	0.13E-3	0.0001	1.8960	0.2143	30912	24563
	0.09	9,32	1	0.22068	0.2205	2.0014	2.0671	661	661
			0.5	0.22068	0.2205	2.0014	2.0671	661	661
			0.1	0.22068	0.2205	2.0014	2.0671	200	201
			0.05	0.22068	0.2205	2.0014	2.0671	200	201

Table 4.2. The smallest values of $FD_{\text{magnitude}}^{\text{FL}}$ and $FD_{\text{magnitude}}^{\text{DWBA}}$ for the different spatial distributions and wavelengths, in the approximate FL and DWBA, from the list LLi ($i = 1,2$). The first three lines contain

the average values of the data obtained for the random multiplicative noise and the last two lines for the white additive Gaussian noise with a variance of 0.01 and 0.1.

P=0 vs. P=0.00009						P=0 vs. P=0.09					
λ	Geometry	$FD_{FL}^{magnitude}$	λ	Geometry	$FD_{DWBA}^{magnitude}$	λ	Geometry	$FD_{FL}^{magnitude}$	λ	Geometry	$FD_{DWBA}^{magnitude}$
0.5	(T)	0.21E-3	0.5	(E)	0.33E-3	1	(T)	0.217	1	(E)	0.345
1	(D)	0.18E-3	1	(P)	0.24E-3	1	(D)	0.183	1	(P)	0.244
1	(D)	0.17E-3	0.5	(E)	0.20E-3	1	(D)	0.174	1	(E)	0.345
0.5	(P)	0.20E-3	1	(D)	0.94E-3	1	(E)	0.020	1	(E)	0.020
0.5	(T)	0.23E-3	0.5	(E)	0.33E-3	1	(D)	0.042	1	(D)	0.062

The FD values for the "Magnitude" curves in both approximations, presented in Table 4.1, show variations with both the wavelength and the spatial geometric distribution of the targets. According to our analysis, the diamond (D) and ellipse (E) geometry have higher FD values for the two approximation models (Table 4.2). "Amplitude" is more influenced by noise. The Foldy-Lax approximation is a model with a better tolerance to noise, while the DWBA model is governed by a more unstable reconstruction process, with the effects of noise in the propagation environment influencing the reconstructed signals.

In the case of simulation experiments aimed at detecting and locating a finite number of targets performed using the Multiple Signal Classification (MUSIC) algorithm using data from the multistatic response matrix, the following conclusions were drawn:

- Two approximations were used: the Foldy-Lax (FL) formulation of the multiple scattering model and the distorted-wave Born approximation (DWBA) model. Fréchet distance is an easy-to-implement tool in an inverse spread optimization algorithm. Optimization is accomplished by minimizing FD values and searching for maximum values of the amplitude of backscattered signals.
- Numerical results show a higher effectiveness of the Foldy-Lax approximation in identifying target locations.
- Our results indicated that the efficiency of target localization depends marginally on the location of internal targets in the chosen geometries, but that it strongly depends on the wavelength and noise level.
- Both approximations work steadily and can tolerate moderate noise.
- The inverse scattering problem has been successfully used to identify multiple target locations, especially for tightly wrapped targets such as diamond and elliptic geometry, with distances between targets having the values λ , $\sqrt{2}\lambda$.

REFERENCE LIST

Articles published in Web of Science, Scopus / ISI Proceedings indexed volumes.

- **Maria (Stan) Necula**, Dorin Bibicu și Luminița Moraru, BACKSCATTERING PROBLEMS BY A NON-CONVEX KITE-SHAPE OBJECTS IN ACOUSTIC FREQUENCY DOMAIN, AIP Conference Proceedings 2071, 040008 (2019); <https://doi.org/10.1063/1.5090075>
- Dorin Bibicu, **Maria (Stan) Necula** și Luminița Moraru, ACOUSTIC RADIATION FROM BAFFLED VIBRATING PLATES WITH VARIOUS GEOMETRIES - SIMULATION RESULTS, AIP Conference Proceedings 2071, 040009 (2019); <https://doi.org/10.1063/1.5090076>
- Dorin Bibicu, **Maria (Stan) Necula** și Luminița Moraru , INVERSE SCATTERING PROBLEM FOR CONCEALED OBJECTS DETECTION, AIP Conference Proceedings 2218, 030007 (2020), <https://doi.org/10.1063/5.0001012>
- **Maria (Stan) Necula**, Dorin Bibicu și Luminița Moraru, ANALYSIS OF BACKSCATTERING DATA FROM CLOSELY SPACED SCATTERERS USING THE K MATRIX INFORMATION, Sensors & Transducers, Vol. 245, Issue 6, pp. 99-104

Articles published in international databases (indexed by EBSCO)

- **Maria (Stan) Necula**, Dorin Bibicu, Simona Moldovanu și Luminita Moraru, Performance analysis of an array of sensors based on the direction of arrival algorithm, ANNALS OF "DUNAREA DE JOS" UNIVERSITY OF GALATI MATHEMATICS, PHYSICS, theoretical mechanics FASCICLE II, YEAR X (XLI) 2018, No. 1, pp 65-69, DOI: <https://doi.org/10.35219/ann-ugal-math-phys-mec.2019.1.06>
- **Maria (Stan) Necula**, Dorin Bibicu, Luminita Moraru, Vibration of rectangular plates: fundamental mode and integer multiple of the fundamental period of vibration, ANNALS OF "DUNAREA DE JOS" UNIVERSITY OF GALATI MATHEMATICS, PHYSICS, THEORETICAL MECHANICS FASCICLE II, YEAR XI (XLII) 2019, No. 1, pp 43-48, DOI: <https://doi.org/10.35219/ann-ugal-math-phys-mec.2019.1.06>
- Maria (Stan) Necula, Dorin Bibicu, Luminita Moraru, Cristian-Victor-Eugen Rusu,, Multiple closely spaced scatterers location based MUSIC via inverse scattering amplitude estimation, ANNALS OF "DUNAREA DE JOS" UNIVERSITY OF GALATI, MATHEMATICS, PHYSICS, THEORETICAL MECHANICS FASCICLE II, YEAR XII (XLIII) 2020, No. 1, pp 1-12, DOI: <https://doi.org/10.35219/ann-ugal-math-phys-mec.2020>

Participation in national and international conferences

1. **Maria (Stan) Necula**, Dorin Bibicu, Luminita Moraru, BACKSCATTERING PROBLEMS BY A NON-CONVEX KITE-SHAPE OBJECTS IN ACOUSTIC FREQUENCY DOMAIN, TIM 18 Physics Conference, 24 - 26 Mai 2018, Timișoara, România
2. Dorin Bibicu, **Maria (Stan) Necula** și Luminita Moraru, ACOUSTIC RADIATION FROM BAFFLED VIBRATING PLATES WITH VARIOUS GEOMETRIES - SIMULATION RESULTS, TIM 18 Physics Conference, 24 - 26 Mai 2018, Timișoara, România
3. Dorin Bibicu, **Maria (Stan) Necula** și Luminița Moraru, INVERSE SCATTERING PROBLEM FOR CONCEALED OBJECTS DETECTION, TIM 19 Physics Conference, 29 - 31 Mai 2019, Timișoara, România
4. **Maria Stan Necula**, Dorin Bibicu and Luminița Moraru, BACKSCATTERING BY CLOSELY SPACED SCATTERERS USING THE K MATRIX DATA FROM AN ACTIVE ARRAY OF N TRANSCIEVERS, 6th International Conference on Sensors Engineering and Electronics Instrumentation Advances (SEIA' 2020), 23-25 September 2020, Porto, Portugal
5. **Maria (Stan) Necula**, Dorin Bibicu, Simona Moldovanu și Luminița Moraru, PERFORMANCE ANALYSIS OF AN ARRAY OF SENSORS BASED ON THE DIRECTION OF ARRIVAL ALGORITHM, 6th edition of the Scientific Conference of the Doctoral Schools of "Dunărea de Jos" University of Galati (SCDS-UDJG), 7-8 iunie 2018, Galați, România.
6. **Maria (Stan) Necula**, Dorin Bibicu și Luminița Moraru, VIBRATION OF RECTANGULAR PLATES: FUNDAMENTAL MODE AND INTEGER MULTIPLE OF THE FUNDAMENTAL PERIOD OF VIBRATION, 7th edition of the Scientific Conference of the Doctoral Schools of "Dunărea de Jos" University of Galati (SCDS-UDJG), 13-14 iunie 2019, Galați, Romania.
7. Dorin Bibicu, **Maria (Stan) Necula**, Luminița Moraru, Cistian-Victor-Eugen Rusu, MULTIPLE CLOSELY SPACED SCATTERERS LOCATION BASED MUSIC VIA INVERSE SCATTERING AMPLITUDE ESTIMATION, 8th edition of the Scientific Conference of the Doctoral Schools of "Dunărea de Jos" University of Galati (SCDS-UDJG), 18-19 iunie 2020, Galați, Romania.

SELECTIVE BIBLIOGRAPHY

55. C. Anand, S. Delrue, H. Jeong, S. Shroff, R. Groves, R. Benedictus, *Simulation of Ultrasonic Beam Propagation From Phased Arrays in Anisotropic Media Using Linearly Phased Multi-Gaussian Beams*, IEEE Transactions on Ultrasonics, Ferroelectrics, and Frequency Control, 67(1), (2020) 106-116, ISSN 0885-3010;
66. S. Magura, S. Petropavlovsky, S. Tsynkov, E. Turkel. *High-order numerical solution of the Helmholtz equation for domains with reentrant corners*. Applied Numerical Mathematics, Volume 118, 2017, Pages 87-116, ISSN 0168-9274
70. H. Ammari, G. Josselin, J. Vincent Jugnon, *Detection, reconstruction and characterization algorithms from noisy data in multistatic wave imaging*, Discrete and Continuous Dynamical Systems, 8 (2015) 389-417, ISSN 1078-0947;
71. A. J. Devaney, E. A. Marengo, F. K. Gruber, *Time-reversal-based imaging and inverse scattering of multiply scattering point targets*, The Journal of the Acoustical Society of America, 118 (2005) 3129–3138, ISSN 0001-4966;
80. E. A. Marengo, R. D. Hernandez, Y. R., Citron, F. K. Gruber, M. Zambrano, H. Lev-Ari, *Compressive sensing for inverse scattering*, General Assembly, 2008, Illinois, ISBN 978-1-4799-3538-3;
81. E. A. Marengo, F. K. Gruber, *Noniterative analytical formula for inverse scattering of multiply scattering point targets*, Journal of the Acoustical Society of America, 120 (2006) 3782–3788, ISSN 0001-4966;
86. D. Ciunzo, G. Romano, R. Solimene, *Performance Analysis of Time-Reversal MUSIC*, IEEE Transactions on Signal Processing, 63 (2015) 2650-2662, ISSN 19410476;
94. G. Shi, A. Nehorai, H. Liu, B. Chen, Y. Wang, *Multiple scattering effects on the localization of two point scatterers*, Proc. IEEE. International Conference on Acoustics, Speech, and Signal Processing (ICASSP), (2016) 3126-3130, ISSN 7367791;
95. D. Ciunzo, P. S. Rossi, *Noncolocated Time-Reversal MUSIC: High-SNR Distribution of Null Spectrum*, IEEE Signal Processing Letters, 24(4), (2017) 397 – 401, ISSN 10709908;
100. M. Moscoso, A. Novikov, G. Papanicolaou, C. Tsogka, *Robust multifrequency imaging with MUSIC*, Inverse Problems, 35(1), (2018), ISSN 0266-5611;
118. Morse P M, Ingard U K, *Theoretical Acoustics*, MCGRAW-HILL BOOK COMPANY, 1968, New York, ISBN 978-0691024011;
119. J. J. Faran, *Sound scattering by solid cylinders and spheres*, The Journal of Acoustical Society of America, 23(4), (1951) 405-418, ISSN 0001-4966;
138. **M. (Stan) Necula**, D. Bibicu, L. Moraru, Backscattering problems by a non-convex kite-shape objects in acoustic frequency domain, AIP Conference Proceedings, 207 (2019); <https://doi.org/10.1063/1.5090075> ;
139. F. K. Gruber, E. A. Marengo, A. J. Devaney, *Time-reversal imaging with multiple signal classification considering multiple scattering between the targets*. Journal of Acoustical Society of America, 115 (2004) 3042-3047, ISSN 0001-4966;

- 140.C. Prada, J. L. Thomas, *Experimental subwavelength localization of scatterers by decomposition of the time-reversal operator interpreted as a covariance matrix*. Journal of the Acoustical Society of America, 114 (2003) 235-243, ISSN 0001-4966;
- 141.T. Miwa, I. Arai, *Super-resolution imaging for point reflectors near transmitting and receiving array*. IEEE Transactions on Antennas and Propagation, 52 (2004) 220-229, ISSN 0018-926x;
- 142.**M. Necula (Stan)**, D. Bibicu, L. Moraru, *Backscattering problems by a non-convex kite-shape objects in acoustic frequency domain*, TIM 18 Physics Conference, Timisoara, Romania, 24 - 26 May 2018;
- 163.H. Lev-Ari, A. J. Devaney, *The time-reversal technique re-interpreted: subspace-based signal processing for multi-static target location*, Proceedings of the 2000 IEEE Sensor Array and Multichannel Signal Processing Workshop. SAM 2000, Cambridge, MA, USA;
- 166.W. K. Park, *Interpretation of MUSIC for Location Detecting of Small Inhomogeneities Surrounded by Random Scatterers*, Mathematical Problems in Engineering, Article 7872548, (2016) 13, ISSN 1024-123X;
- 167.W. K Park, *Asymptotic properties of MUSIC-type imaging in two-dimensional inverse scattering from thin electromagnetic inclusions*, SIAM Journal on Applied Mathematics, 75(1), (2015) 209–228, ISSN 00361399;
- 174.A. G. Ramm, S. Gutman, *Optimization methods in direct and inverse scattering*, *Optimization Methods in Direct and Inverse Scattering*, Continuous Optimization. Applied Optimization; Jeyakumar, V., Rubinov A., Eds.; Springer, Boston, 99 (2005);